Evaluation and development of methods for time-frequency analysis of heart rate variability

Isabella Reinhold

Master's thesis
2015:E32

Lund University

Faculty of Engineering
Centre for Mathematical Sciences
Mathematical Statistics

Centrum Scientiarum Mathematicarum

Abstract

Non-stationary signals are very common in nature, consider for example speech, music or heart rate. Using the concept of time-frequency analysis this thesis studies the performance of different time-frequency distributions of both simulated and real non-stationary signals. The signals studied are linear and non-linear frequency modulated (FM) signals. Two methods are studied to increase performance of the signals' time-frequency distributions. Since lag-independent kernels perform well with slow varying frequency modulated signals both methods use these. One method uses filtering with compact support lag-independent kernels and the other uses a penalty function with multitapers corresponding to lag-independent kernels. These methods are then evaluated using two performance measures and the results are used to improve the time-frequency distributions of heart rate variability signals. The thesis suggests that both of these methods improve the time-frequency distribution of such signals.

Acknowledgements

I wish to express my sincere thanks to my supervisor Professor Maria Sandsten at Mathematical Statistics at Lund University for her support and guidance. Her continuous encouragement has increased my interest in the field of time-frequency analysis and motivated me throughout my work.

I would also like to thank everyone who shared our office during the past six months. Especially Maria Juhlin who has provided invaluable advice and support, as well as making the office a much livelier place filled with interesting discussions and weird music.

Finally I would like to express my heartfelt gratitude towards my family and friends who have been understanding and supportive during not only the last six months but the past five years. This would in no way be possible without them.

Popularised summary

In nature signals which vary in frequency with time are very common. These can be found in for example speech, music or heart rate. The change in frequency over time and what frequencies exist in these signals is hard to detect when only looking at the signal as a function of time. It is also possible to look at the signal as a function of frequency, to see the frequency content of the signal. Methods to do this are simple and accurate, however it is not possible to see when in time the frequencies occur. This means that very different signals can look the same when described as a function of frequency.

Naturally this means that there is a need to look at the signal with respect to time and frequency at the same time. This is however not always easy, especially if the signal has two components. Imagine for example if two people speak at the same time or two musical instruments play at same time. The purpose of this thesis is to look at two relatively new methods more accurately describing two-component signals in time and frequency simultaneously. One of the methods was adapted to better suit the signals analysed and both methods were applied to different signals than they were originally proposed to be used on. These things make the results of this thesis interesting.

The methods are initially tested on simulated, i.e. known, signals to be able to assess their performance. The initial results were very promising so the methods were also applied to real signals. These signals were so called heart rate variability (HRV) signals, which essentially is the difference in time between different heartbeats. These signals can be measured using ECG and can for example be used to see if the health of a person is compromised. Since this is a non-invasive way of monitoring a person's health, finding a way to accurately describe them in time and frequency simultaneously is needed.

The result for the HRV signals was less conclusive than for the simulated signals. This is mostly because only two examples were studied, more HRV signals would be needed to say something definite. Another factor which contributed to the inconclusive results is that it is difficult to assess which representation of the signal that is the best. This is unfortunately a large issue with looking at a signal in both time and frequency.

This thesis proposes an improved method of automatically and objectively asses performance of a joint time-frequency representation of a signal. This method is shown to be more successful in automatically capturing the necessary characteristics to assess performance than the existing method it is based on. The improved method works very well on simulated signals. It is not as successful with the real HRV signal, but this is a far more complex problem and perfect automatic detection might not be possible.

In conclusion this thesis shows that the two analysed methods improve time-frequency representations of the simulated signals. Which suggest that the methods should work well on similar and unknown signals. Further testing on HRV signals are needed to be able to say if any of the two methods will give better results. The testing on simulated signals, one which resembles the HRV signal, suggests that the methods would be successful in improving performance.

Contents

Abbreviations and notations

$A_z(\nu,\tau)$	Ambiguity function for signal $z(t)$
$A_z^g(\nu,\tau)$	Filtered ambiguity function for signal $z(t)$
CD	Cauchy distribution
CS	Compact support
IAF	Instantaneous auto-correlation function
IF	Instantaneous frequency
f	Frequency
$\mathcal{F}\{\cdot\}$	Fourier transform
$\Phi(t,f)$	Time-frequency kernel
FM	Frequency modulated
$g(\nu,\tau)$	Doppler-lag kernel
$G(t,\tau)$	Time-lag kernel
$G_1(\nu)$	Lag-independent kernel
HRV	Heart rate variability
$K_z(t,\tau)$	Instantaneous auto-correlation function for signal $z(t)$
LID	Lag-independent
MBD	Modified B-distribution
MSE	Mean squared error
ν	Doppler, frequency lag
$\Re\{\cdot\}$	Real part
$\rho_z(t,f)$	Time-frequency distribution for signal $z(t)$
$S_z(t,f)$	Spectrogram for signal $z(t)$
t	Time
τ	Time lag
TFD	Time-frequency distribution
WVD	Wigner-Ville distribution
$W_z(t,f)$	Wigner-Ville distribution for signal $z(t)$
$[\cdot]^*$	Complex conjugate
$[\cdot]*[\cdot]$	Convolution

1 Problem presentation

Time-frequency analysis is used for signals which vary both in time and frequency, i.e. non-stationary and time-varying signals. These signals are common in nature, consider for example speech, music or heart rate. All the characteristics of these signals can not be seen from a time or frequency representation only. There is thus a need to view such signals in time and frequency domain simultaneously. In time-frequency analysis the variables time and frequency are not treated as mutually exclusive, as with time-domain and frequency-domain representations of a signal, they are instead used concurrently. The advantage of time-frequency analysis is easily realised when studying the signals in Figure 1. Figure 1a) shows a linear frequency modulated (FM) signal and Figure 1b) a Gaussian component signal, we can see that these are obviously not the same. However when studying their periodograms Figures 1c) and d) it is hard to tell them apart. From the time-domain representations of the signals it is thus not possible to see the frequency content of the signals and from the frequency-domain representation it is not possible to determine how non-stationary signals change with time.

To show the time and frequency content of a signal simultaneously, a distribution which has a two-dimensional domain is sought after, such a representation is called a time-frequency distribution (TFD). Figure 2 shows TFDs of the same signals as in Figure 1. The time and frequency varying behaviour of the signals can now be studied and it is clear from their time-frequency representations that the signals are different.

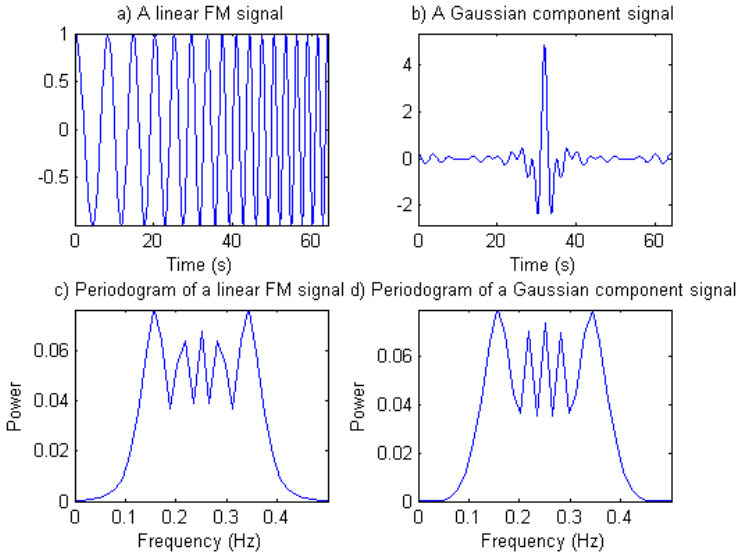

Figure 1: Separate time and frequency representations of two signals. a) A time-domain representation of a linear FM signal. c) A frequency-domain representation of the same signal. b) A time-domain of a Gaussian component signal. d) A frequency-domain representation of the same signal. Both signals have duration 64 seconds and are sampled at a rate of 8 Hz.

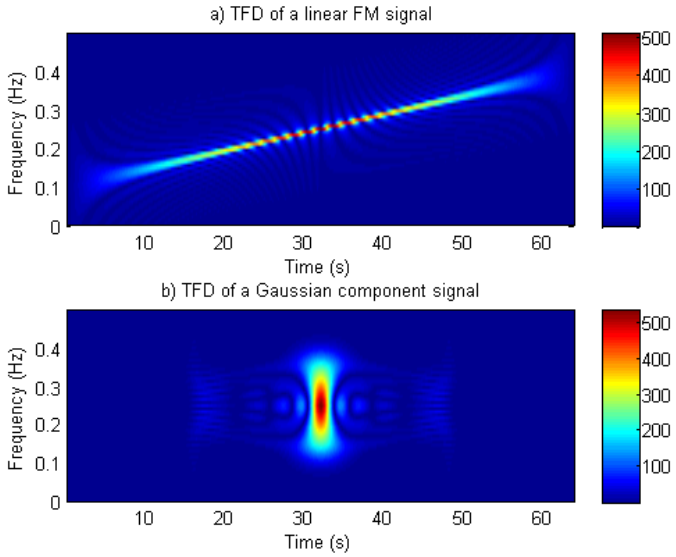

Figure 2: a) A time-frequency representation a linear FM signal. b) A time-frequency representation of a Gaussian component signal. Both signals have duration 64 seconds and are sampled at a rate of 8 Hz.

There are many types of non-stationary signals. This thesis will further study two recently published methods for improving the TFDs of slow varying FM signals. For both the studied methods so called lag-independent kernels will be used, these kernels are especially suited to use with slow varying FM signals, which will be shown later. This thesis will first evaluate the performance of TFDs for simulated, relatively slow varying FM signals. The signals considered will have two components. These signals are studied because they resemble heart rate variability (HRV) data. FM signals with both linear and non-linear components will be assessed. A linear FM signal is a signal whose components are either constant in frequency (stationary) or vary linearly in frequency over time. A non-linear FM signal has at least one component which varies non-linearly in frequency over time. The non-linear FM signal is considered because is very closely resembles the actual HRV data obtained from a few patients which have been asked to breathe with the same frequency as a metronome. The metronome increases frequency non-linearly which gives a non-linear component.

Heart rate variability, which is the variation of inter-heartbeat intervals, is measured non-invasively using ECG. It provides information on the autonomic regulation of the cardiovascular system. This means that the HRV is a sensitive indicator of compromised health [1], [2]. Many methods for assessing HRV with assumption of stationary exist, however these methods are not always sufficient and good TFDs of HRV are needed [3]. The hope is that the methods investigated in this thesis will provide better TFDs for HRV signals.

The thesis is organised as follows. Section 2 provides an introduction to the basics of time-frequency analysis and what difficulties it entails. Section 3 explains the concept of ambiguity functions and introduces the lag-independent kernel as a means of overcoming some of the difficulties with time-frequency analysis. In Section 4 two methods for objectively assessing the performance of TFDs are described. The two methods which aim to improve TFDs for slow

varying FM signals are described in Sections 5 and 6. The performance of the two analysed methods for one linear and one non-linear FM signal is evaluated in Section 7. In Section 8 the performance of the two methods on examples of real HRV data is demonstrated. Sections 9 and 10 conclude the thesis.

2 Introduction to time-frequency analysis

In this section the area of time-frequency analysis will be further explained. Some basic time-frequency distributions (TFDs) will be introduced as well as their relationship. The largest challenges with time-frequency analysis will also be discussed.

2.1 Some desired characteristics of a TFD

There is a need to accurately represent non-stationary signals in the time-frequency plane. Several methods to do this have been developed and still new methods are developed. This is because for some signals, especially multi-component signals, it is difficult to obtain a good TFD. Naturally this means that there needs to be a definition, or at least a sense, of what a good TFD is. No single method of obtaining the TFD is the best for all signals or situations, however some desirable characteristics are listed below, these and more characteristics are found in [4], [5] and [6].

1. The TFD should be real valued.
2. The integral of the TFD, over the entire time-frequency plane, should be the total energy of the signal.
3. For a mono-component FM signal, the peaks of the constant-time cross-sections of the TFD should give the instantaneous frequency (IF) law which describes the signal FM law. This means that the energy concentration of the TFD at a given time should be highest at the frequency where the signal has a component.
4. For a multi-component FM signal, the dominant peaks of the TFD should reflect the components respective FM laws.
5. For a multi-component FM signal the TFD should resolve any close components.
6. The TFD should be time and frequency invariant.

These desired characteristics can be used to implement performance measures, which will allow for comparison between different TFDs. This will be discussed further in Section 4.

2.2 The Wigner-Ville distribution

The Wigner-Ville distribution (WVD) is a commonly used TFD, it is defined using an analytic signal. An analytic signal is a signal $z(t)$ such that $Z(f) = 0$ if $f < 0$, where $Z(f) = \mathcal{F}\{z(t)\}$, the Fourier transform of the signal. If one wants to use a non-analytic (real valued) signal it is instead possible to get the Wigner distribution (see [7] for further reading). One advantage of using an analytic signal is that the TFD will be easier to interpret. The analytic signal can be obtained from any real valued signal using the Hilbert transform [7].

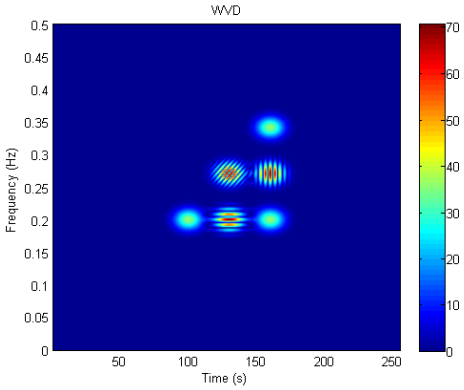

Figure 3: The WVD of a three-component signal with duration 256 seconds and sampling rate 2 Hz. The signal has components at $f = 0.20$ for $t = 100$ and $t = 160$ and $f = 0.34$ for $t = 160$.

The WVD is defined as

$$W_z(t,f) = \int_{-\infty}^{\infty} z\left(t+\tfrac{\tau}{2}\right) z^*\left(t-\tfrac{\tau}{2}\right) e^{-i2\pi f\tau} d\tau, \tag{1}$$

where * represents the complex conjugate of the analytic signal $z(t)$. Notice also that $K_z(t,\tau) = z\left(t+\frac{\tau}{2}\right) z^*\left(t-\frac{\tau}{2}\right)$ is an estimate of the auto-correlation function of $z(t)$ and is called the instantaneous auto-correlation function (IAF). This means that the WVD is the Fourier transform of the estimated IAF. Therefore, for mono-component signals, the WVD gives exactly the IF and thus fulfils the 3rd characteristic in Section 2.1. In fact the WVD is optimal for mono-component signals since it, compared to all other TFDs, achieves the best energy concentration around the signal IF law [5], [8].

The WVD also fulfils the 2nd characteristic in Section 2.1, i.e. the integral over $W_z(t,f)$ is the total energy of the signal. However a problem with the WVD occurs when dealing with multi-component signals or signals with noise. For such a signal the WVD is not always zero when the signal has no frequency contribution at a given time. This phenomenon is called cross-terms and makes is difficult to interpret the WVD, cross-terms will be discussed further in Section 2.4. The WVD of a three-component signal can be seen in Figure 3. The signal has components at $f = 0.20$ for $t = 100$ and $t = 160$ and $f = 0.34$ for $t = 160$ and we can clearly see the cross-terms in between all signal components, so called auto-terms.

2.3 The spectrogram

Another frequently used way to represent a signal in the time-frequency domain is to calculate its spectrogram. The spectrogram is calculated by dividing the signal into several short segments and estimating the spectrum [7] for all, often overlapping, segments. This could be done using the short-time Fourier transform (STFT), which is defined as

$$X(t,f) = \int_{-\infty}^{\infty} x(t_1) h^*(t-t_1) e^{-i2\pi f t_1} dt_1, \tag{2}$$

where $x(t)$ is the (real valued or analytic) signal and $h(t)$ a real, even window function centred at time t. The introduction of the window function essentially means that the Fourier transform will

be estimated locally around several time instants. Usually $h(t)$ is a fixed, positive window with some predetermined shape, which is centred around 0 and has the power 1. The spectrogram of the signal $x(t)$ is then

$$S_x(t,f) = |X(t,f)|^2. \tag{3}$$

The spectrogram has a fast implementation and is very easily related to the periodogram, it also doesn't suffer from cross-terms. The problem with the spectrogram lies with choosing an appropriate window and window length. The spectrogram also has difficulties resolving components in multi-component signals which are close in both time and frequency, as there is a trade-off between time and frequency resolution. If the components of a signal are close together the leakage between the signal components can occur, similar to cross-terms.

The importance of choosing the right window length and the trade-off between resolution in frequency and time is clearly shown i Figure 4. In Figure 4a) the window length is long which results in poor resolution in time, in Figure 4b), with shorter window length, the time and frequency resolution is approximately the same and for a short window length, shown in Figure 4c) there is poor resolution in frequency. Notice also the absence of cross-terms, which is the large problem with the WVD (Figure 3), however there is leakage between the two components at $f = 0.20$ in Figure 4a) and the components at $t = 160$ in Figure 4c). Additionally all window lengths result in poorer resolution, or smoothing, of the auto-terms when compared to the WVD.

2.4 Cross-terms

The existence of cross-terms in the WVD is due to that it is quadratic in the signal, i.e. the signal is squared when calculating the TFD. The spectrogram is also quadratic in the signal, however the non-linearity is introduced only in the final calculation step. This is the reason why the spectrogram doesn't suffer from cross-terms, the leakage in spectrograms is however due to its quadratic nature and exist only when the signal components are too close to each other to be properly resolved.

Cross-terms make the WVD hard to interpret, especially when the signal has numerous components or if they are close together, the difficulty also increases in the presence of noise. Cross-terms are always located midway between two components of a signal, indifferent of the distance between the components, and can have twice the magnitude of the auto-terms. If we assume an analytic signal has two components $z(t) = x(t) + y(t)$, then the WVD will be

$$W_z(t,f) = W_x(t,f) + W_y(t,f) + 2\Re\left\{W_{x,y}(t,f)\right\}, \tag{4}$$

where $W_x(t,f)$ and $W_y(t,f)$ are the WVD of the two signals $x(t)$ and $y(t)$, the auto-terms, and $2\Re\left\{W_{x,y}(t,f)\right\}$ is the cross-term. Observe that

$$W_{x,y}(t,f) = \int_{-\infty}^{\infty} x\left(t+\tfrac{\tau}{2}\right) y^*\left(t-\tfrac{\tau}{2}\right) e^{-i2\pi f\tau} d\tau. \tag{5}$$

Much research has been devoted to the suppression of cross-terms and a large area revolves around time-frequency kernels. These time-frequency kernels are often designed in something called the ambiguity or Doppler-lag domain, where the auto- and cross-terms can be more easily distinguished from one another. Section 3 will further discuss the ambiguity domain and cross-term suppression using different time-frequency kernels.

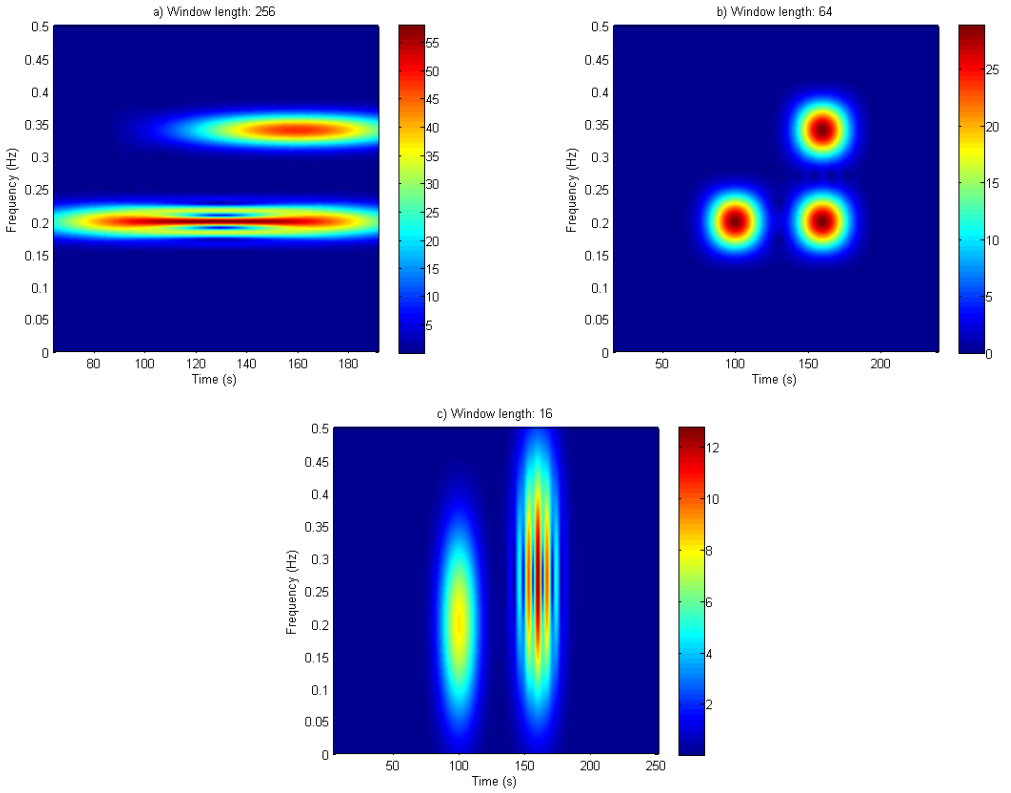

Figure 4: The spectrogram of a three-component signal with duration 256 seconds and sampling rate 2 Hz. The signal has components at $f = 0.20$ for $t = 100$ and $t = 160$ and $f = 0.34$ for $t = 160$. a) The spectrogram with window length 256 samples. b) The spectrogram with window length 64 samples. c) The spectrogram for with window length 16 samples.

The cross-terms discussed above arise from a signal having multiple components. The TFD of a mono-component signal can however also have disturbance. If the signal is non-linear the WVD will have so called inner artifacts, sometimes called inner cross-terms. A non-linear signal is here referred to a signal which vary non-linearly in frequency over time. Figure 5 shows this phenomenon for a non-linear FM signal. The inner artifacts can be seen in the time interval 40-100 seconds, they are the strong waves/ridges in the curve of the signal. Inner artifacts can be removed by windowing the WVD, however this results in loss of frequency resolution [5].

2.5 Relationship between the WVD and the spectrogram

The WVD and the spectrogram are both so called quadratic TFDs, this means that they are quadratic in the signal. However these two TFDs are also further related. The instantaneous auto-correlation function (IAF) of an analytic signal was briefly introduced in Section 2.2, when calculating the WVD. It was defined as

$$K_z(t,\tau) = z\left(t+\tfrac{\tau}{2}\right) z^*\left(t-\tfrac{\tau}{2}\right). \tag{6}$$

With the introduction of a time-lag kernel $G(t,\tau)$ it is possible to write both the WVD and the spectrogram as Fourier transforms of the convolution (in time) $G(t,\tau) \underset{t}{*} K_z(t,\tau)$. Since the WVD

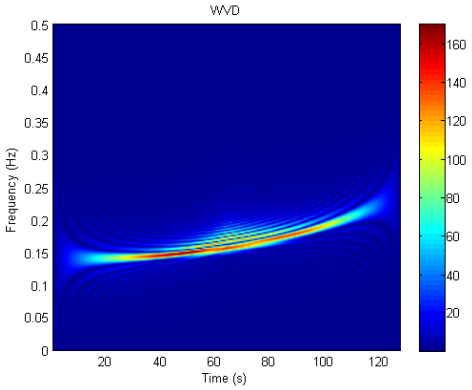

Figure 5: The WVD of a mono-component signal with duration 128 seconds and sampling rate 2 Hz. The signal component starts at frequency 0.14 Hz and then increases non-linearly to frequency 0.24 Hz.

is calculated directly from the Fourier transform of $K_z(t,\tau)$, clearly the kernel is $G(t,\tau)=\delta(t)$.

Finding the kernel for the spectrogram requires more calculations. Using the definition of the spectrogram with an analytic signal $z(t)$ it is possible to write

$$\begin{aligned} S_z(t,f) &= \left| \int_{-\infty}^{\infty} z(t_1)h^*(t-t_1)e^{-i2\pi f t_1}dt_1 \right|^2 \\ &= \int_{-\infty}^{\infty} z(t_1)h^*(t-t_1)e^{-i2\pi f t_1}dt_1 \left(\int_{-\infty}^{\infty} z(t_2)h(t-t_2)e^{-i2\pi f t_2}dt_2 \right)^* \\ &= \int_{-\infty}^{\infty}\int_{-\infty}^{\infty} z(t_1)h^*(t-t_1)z^*(t_2)h(t-t_2)e^{-i2\pi f(t_1-t_2)}dt_1dt_2. \end{aligned} \tag{7}$$

With the variable changes $t_1 = u+\frac{\tau}{2}$ and $t_2 = u-\frac{\tau}{2}$ the convolution can be written

$$\begin{aligned} S_z(t,f) &= \int_{-\infty}^{\infty}\int_{-\infty}^{\infty} h(t-u+\tfrac{\tau}{2})h^*(t-u-\tfrac{\tau}{2})z(u+\tfrac{\tau}{2})z^*(u-\tfrac{\tau}{2})e^{-i2\pi f\tau}dud\tau \\ &= \int_{-\infty}^{\infty} \Big(h(t+\tfrac{\tau}{2})h^*(t-\tfrac{\tau}{2})\Big) \underset{t}{*} \Big(z(t+\tfrac{\tau}{2})z^*(t-\tfrac{\tau}{2})\Big)e^{-i2\pi f\tau}d\tau, \end{aligned} \tag{8}$$

the second equality uses the evenness of the window function $h(t)$. This means that the time-lag kernel for the spectrogram is $G(t,\tau)=h(t+\frac{\tau}{2})h^*(t-\frac{\tau}{2})$.

There exist more quadratic TFDs than the WVD and the spectrogram, lets call all those TFDs $\rho_z(t,f)$. These TFDs can then be written as

$$\rho_z(t,f) = \int_{-\infty}^{\infty} G(t,\tau) \underset{t}{*} K_z(t,\tau)e^{-i2\pi f\tau}d\tau, \tag{9}$$

where the time-lag kernel $G(t,\tau)$ is specific for each different quadratic TFD and $K_z(t,\tau)$ is the IAF of the analytic signal $z(t)$. Some historically important and popular TFDs can be found in [7] and [8]. The convolution $G(t,\tau) \underset{t}{*} K_z(t,\tau)$ can be seen as a smoothing of the TFD compared to the WVD.

2.6 Transition to discrete calculations with finite signals

All the above definitions and calculations assume that the considered signal is continuous and infinite. For the calculations of TFDs for both simulated and real measured signals, this is however not the case. The integrals are then approximated by sums and the Fourier transforms with Fast Fourier transforms. This impacts the estimated TFD.

Using finite length signals means that the signal components will be smoothed near the edges of the TFD. There will also be some smoothing in time and frequency due to the signal not being continuous. Too improve resolution of the TFD zero padding is used with the Fast Fourier transform. Zero padding increases the length of the signal and thus calculations can be done using more bins which increases the resolution.

It is also important to sample any measured signal with sufficiently high sampling frequency. The sampling frequency should be at least twice the highest frequency of the signal to avoid aliasing, as the TFD for an analytic signal shows frequencies within the range 0 to 0.5.

3 Ambiguity domain and cross-term suppression

The IAF $K_z(t,\tau)$ of an analytic signal $z(t)$ has two variables, time t and time lag τ. The WVD is obtained by calculating the Fourier transform ($\tau \to f$) of the IAF. Introducing the new variable ν, representing frequency lag, called Doppler, it is now possible to calculate the Fourier transform ($t \to \nu$) to get

$$A_z(\nu,\tau) = \int_{-\infty}^{\infty} K_z(t,\tau) e^{-i2\pi t\nu} dt = \int_{-\infty}^{\infty} z\left(t+\tfrac{\tau}{2}\right) z^*\left(t-\tfrac{\tau}{2}\right) e^{-i2\pi\nu t} dt, \tag{10}$$

this is called the ambiguity function of the signal $z(t)$. Note that the ambiguity function is usually calculated using an analytic signal, however a real signal could also be used without any restrictions. This introduces the new domain called the ambiguity or Doppler-lag domain, which is the plane represented by the two variables (ν,τ). Using the ambiguity domain it is possible design kernels to suppress cross-terms of the WVD.

3.1 Cross-term suppression

In the ambiguity domain it is less hard, though not always easy, to distinguish auto-terms from cross-terms. The auto-terms of a signal is always located near the origin of the ambiguity function and the cross-terms are always symmetrically located at a distance from the origin, which is equal to the time-frequency distance between the interacting signal components [9]. This gives the opportunity to suppress cross-terms by multiplying the ambiguity function with some other function, namely a kernel. The ambiguity function of a three-component signal can be seen in Figure 6. In the figure the different placement of the auto- and cross-terms can be clearly observed. The signal has components at $f = 0.1$ for $t = 80$ and $t = 170$ and $f = 0.3$ for $t = 170$ and its WVD and spectrograms are shown in Figures 3 and 4 respectively.

The concept of the time-lag kernel $G(t,\tau)$ presented in Section 2.5 can naturally be expanded to the ambiguity domain. Lets call the Doppler-lag kernel $g(\nu,\tau) = \underset{t\to\nu}{\mathcal{F}}\{G(t,\tau)\}$. This means that all quadratic TFDs can be formulated as

$$A_z^g(\nu,\tau) = g(\nu,\tau) A_z(\nu,\tau), \tag{11}$$

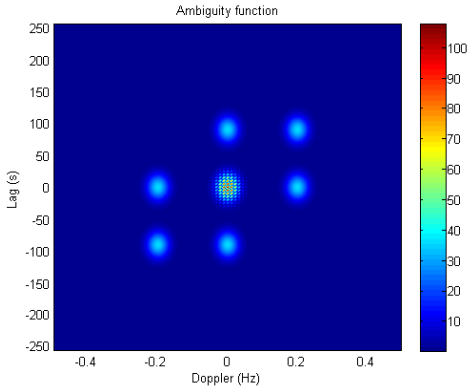

Figure 6: The ambiguity function of a three-component signal with duration 256 seconds and sampling rate 2 Hz. The signal has components at $f = 0.1$ for $t = 80$ and $t = 170$ and $f = 0.3$ for $t = 170$.

and $g(\nu, \tau)$ can be designed to suppress components which are located some distance from the origin of the ambiguity function. The resulting ambiguity function $A_z^g(\nu, \tau)$ is called the filtered ambiguity function, since multiplication with the kernel is (in most cases) equal to a 2D filtering. Although the kernels are usually designed due to their properties in the ambiguity domain, it is also interesting to consider the time-frequency kernel $\Phi(t, f) = \underset{\tau \to f}{\mathcal{F}}\{G(t, \tau)\}$. Note that the following relationships hold

$$\begin{aligned} \rho_z(t, f) = \Phi(t, f) \underset{t,f}{**} W_z(t, f) &= \int_{-\infty}^{\infty} G(t, \tau) \underset{t}{*} K_z(t, \tau) e^{-i2\pi f \tau} d\tau \\ &= \int_{-\infty}^{\infty} \int_{-\infty}^{\infty} g(\nu, \tau) A_z(\nu, \tau) e^{-i2\pi(f\tau - t\nu)} d\tau d\nu. \end{aligned} \tag{12}$$

3.2 General design of Doppler-lag kernels

From the ambiguity function displayed in Figure 6 it might seem a simple problem to suppress the cross-terms using a Doppler-lag kernel. Since the Doppler-lag kernel is multiplied with the ambiguity function an obvious solution would be to set the kernel to 1 in the area of the auto-term and 0 everywhere else. This kernel will work rather well for the signal in Figure 6 if the goal is to identify the locations of the auto-terms. However the resulting TFD will no longer have the property that the integral over the entire time-frequency plane will be equal to the energy of the signal, which is important in some applications. More complex signals also result in more complex ambiguity functions, with auto- and cross-terms being located very close to one another or they might even overlap. All Doppler-lag kernels, except the one which equals 1 everywhere, smooths the TFD, this is why sometimes the TFD obtained from the filtered ambiguity function is called the smoothed WVD. The smoothing, or smearing, is seen in the TFD as sinusoidal ringing. There exists no perfect Doppler-lag kernel for all signals and much research is still dedicated to finding cross-term reducing kernels.

3.2.1 Constraints on the Doppler-lag kernel

Section 2.1 lists some desired characteristics of a TFD, these characteristics, and many more [4], [5], [6], impose requirements on the Doppler-lag kernels for quadratic TFDs. Worth noting is that there are many desired characteristics of a TFD and no known TFD fulfils them of all, this also means that there is no known Doppler-lag kernel which fulfils all constraints. For more details on and a full list of desired characteristics and restraints see [5], [6]. Here follows a list of some of the desired characteristics of a TFD listed in Section 2.1 and what restraints they impose on the Doppler-lag kernel.

1. **Characteristic:** The TFD is real, $\rho_z(t,f) \in \mathbb{R}$.

   Restriction: $g(\nu,\tau) = g^*(-\nu,-\tau)$.

2. **Characteristic:** The integral of the TFD, over the entire time-frequency plane should be the total energy of the signal.

   Restriction: $g(\nu,0) = 1, \forall\nu$ and $g(0,\tau) = 0, \forall\tau$.

3. **Characteristic:** For a mono-component FM signal, the peaks of the constant-time cross-sections of the TFD should give the IF law which describes the signal FM law.

   Restriction: $g(\nu,0) = 1, \forall\nu$ and $\frac{\partial g(\nu,\tau)}{\partial\tau}\big|_{\tau=0} = 0, \forall\nu$.

4. **Characteristic:** Reduced interference in TFD (from ideal characteristic that a multi-component FM signal the TFD should resolve any close component).

   Restriction: The Doppler-lag kernel is a 2D low pass filter type.

5. **Characteristic:** The TFD is time and frequency invariant.

   Restriction: The Doppler-lag kernel does not depend on t or f.

3.3 Lag-independent kernels

One simple, yet useful, class of Doppler-lag kernels is the separable kernel. The separable kernel can be written

$$g(\nu,\tau) = G_1(\nu)g_2(\tau), \tag{13}$$

and gives the following filtered ambiguity function

$$A_z^g(\nu,\tau) = G_1(\nu)g_2(\tau)A_z(\nu,\tau). \tag{14}$$

This means that the design of the kernel will be greatly simplified, the 2D filtering operation is replaced by two consecutive 1D filtering operations. The calculations of the resulting TFD is also simplified, the convolutions in time and frequency can now be done in either order. The TFD is

$$\rho_z(t,f) = g_1(t) \underset{t}{*} W_z(t,f) \underset{f}{*} G_2(f), \tag{15}$$

where

$$G_1(\nu) = \underset{t\to\nu}{\mathcal{F}}\{g_1(t)\}, \quad G_2(f) = \underset{\tau\to f}{\mathcal{F}}\{g_2(\tau)\}. \tag{16}$$

A special case of the separable kernel is the lag-independent (LID) kernel. It is obtained by setting

$$g_2(\tau) = 1, \quad G_2(f) = \delta(f), \tag{17}$$

which means that the Doppler-lag kernel only will depend on Doppler ν

$$g(\nu, \tau) = G_1(\nu). \tag{18}$$

Of course this means that we obtain the filtered ambiguity function by applying only one 1D filtering and the TFD is calculated using only one convolution, in the time direction only

$$\begin{aligned} A_z^g(\nu, \tau) &= G_1(\nu) A_z(\nu, \tau), \\ \rho_z(t, f) &= g_1(t) \underset{t}{*} W_z(t, f). \end{aligned} \tag{19}$$

3.3.1 Characteristics associated with the LID kernel

The LID kernel fulfils some of the constraints listed in Section 3.2.1, which means that the resulting TFD have some characteristics. These characteristics and restrictions are listed below, more details and properties are listed in [5].

1. **Characteristic:** The TFD is real, $\rho_z(t, f) \in \mathbb{R}$.

   Restriction: Lag-independent time kernel is real, $g_1(t) \in \mathbb{R}$.

2. **Characteristic:** Reduced interference in TFD.

   Restriction: None, but only applicable cross-terms between signal components with different frequencies. Does not reduce inner artifacts.

3. **Characteristic:** The TFD is time and frequency invariant.

   Restriction: Lag-independent Doppler kernel, $G_1(\nu)$, does not depend on t or f.

Also since the LID kernel only applies a 1D filtering, the resulting TFD will only be smoothed in the time direction only. This property makes the LID kernel suitable for slowly varying FM signals or other signals where cross-terms exist mainly some frequency distance from the auto-terms and single auto-terms do not vary much in frequency. For such signals auto-terms will be located close to $\nu = 0$ and cross-terms some distance away from $\nu = 0$. For signals which vary much in frequency, i.e. broadband signals, the auto-terms will deviate much from $\nu = 0$ in the ambiguity domain. This means that the LID kernel will notably suppress auto-terms, which is unwanted. Other types of kernels should thus be used with broadband signals. However for the purpose of this thesis slow varying FM signals are of interest and the concept of LID kernels will be further explored.

3.3.2 Application of the LID kernel

The LID kernel works well on some signals but not on others, this section will demonstrate this with calculation of the filtered ambiguity function for two different multi-component signals. The first signal is with two components at different frequencies, this is a signal for which the LID kernel should be able to suppress the cross-terms and keep the auto-terms. The signal can be written

$$z_1(t) = e^{i2\pi f_0 t} + e^{i2\pi f_1 t}. \tag{20}$$

Note that the signal is analytic if $f_0 > 0$ and $f_1 > 0$. The WVD of this signal is

$$\begin{aligned} W_{z_1}(t,f) &= \int_{-\infty}^{\infty} \left(e^{i2\pi f_0\left(t+\frac{\tau}{2}\right)} + e^{i2\pi f_1\left(t+\frac{\tau}{2}\right)}\right)\left(e^{i2\pi f_0\left(t-\frac{\tau}{2}\right)} + e^{i2\pi f_1\left(t-\frac{\tau}{2}\right)}\right)^* e^{-i2\pi f\tau} d\tau \\ &= \int_{-\infty}^{\infty} \left(e^{i2\pi f_o\tau} + e^{i2\pi f_1\tau} + \left(e^{i2\pi t(f_1-f_0)} + e^{i2\pi t(f_0-f_1)}\right) e^{i\pi\tau(f_0+f_1)}\right) e^{-i2\pi f\tau} d\tau \\ &= \delta(f-f_0) + \delta(f-f_1) + 2\delta\left(f - \tfrac{f_0+f_1}{2}\right)\cos(2\pi(f_0-f_1)t). \end{aligned} \tag{21}$$

Figure 7a) shows the WVD for the signal $z_1(t)$ with $f_0 = 0.1$ and $f_1 = 0.3$, the figure clearly shows the auto-term at the correct frequencies and the cross-term in the middle of them. The ambiguity function for $z_1(t)$ is

$$\begin{aligned} A_{z_1}(\nu,\tau) &= \int_{-\infty}^{\infty} \left(e^{i2\pi f_0\left(t+\frac{\tau}{2}\right)} + e^{i2\pi f_1\left(t+\frac{\tau}{2}\right)}\right)\left(e^{i2\pi f_0\left(t-\frac{\tau}{2}\right)} + e^{i2\pi f_1\left(t-\frac{\tau}{2}\right)}\right)^* e^{-i2\pi\nu t} dt \\ &= \int_{-\infty}^{\infty} \left(e^{i2\pi f_o\tau} + e^{i2\pi f_1\tau} + \left(e^{i2\pi t(f_1-f_0)} + e^{i2\pi t(f_0-f_1)}\right) e^{i\pi\tau(f_0+f_1)}\right) e^{-i2\pi\nu t} dt \\ &= \delta(\nu)\left(e^{i2\pi f_0\tau} + e^{i2\pi f_1\tau}\right) + \left(\delta(\nu+(f_0-f_1)) + \delta(\nu-(f_0-f_1))\right) e^{i\pi(f_0+f_1)\tau}. \end{aligned} \tag{22}$$

This means that the auto-term will be located at $\nu = 0$ and the two cross-terms at $\nu = \pm(f_0 - f_1)$ in the ambiguity domain. The ambiguity function of the signal with $f_0 = 0.1$ and $f_1 = 0.3$ is shown in Figure 7b), the auto-term is indeed located at $\nu = 0$ and the cross-terms at $\nu = \pm 0.2$.

Now lets define a LID kernel which is Cauchy distributed (CD)

$$G_{\mathrm{cd}}(\nu) = e^{-\gamma|\nu|}, \quad v \in \mathbb{R}. \tag{23}$$

Figure 7c) shows this LID kernel with $\gamma = 75$. If this kernel is multiplied with the ambiguity function of the signal $z_1(t)$ above, the resulting TFD will be

$$\begin{aligned} \rho_{z_1}(t,f) &= \int_{-\infty}^{\infty}\int_{-\infty}^{\infty} G_{\mathrm{cd}}(\nu) A_{z_1}(\nu,\tau) e^{-i2\pi(\tau f-\nu t)} d\tau d\nu \\ &= \delta(f-f_0) + \delta(f-f_1) + 2\delta\left(f - \tfrac{f_0+f_1}{2}\right) e^{-\gamma|f_0-f_1|}\cos(2\pi(f_0-f_1)t). \end{aligned} \tag{24}$$

Full calculations are shown in Appendix A. The results show that the cross-term will still be present, however suppressed by the factor $e^{-\gamma|f_0-f_1|}$, so if γ is chosen large enough, the cross-term will hardly be noticeable. Figure 7d) shows such a TFD for the signal with $f_0 = 0.1$ and $f_1 = 0.3$ and for the LID kernel with $\gamma = 75$, the cross-term can not really be seen.
The other signal to be examined is a signal with two components at different times, which can be written

$$z_2(t) = \delta(t-t_0) + \delta(t-t_1). \tag{25}$$

This signal is analytic only if frequencies $f < 0$ are ignored. The calculation of the WVD of the signal uses the fact a signal $z(t) = \delta(t-t_0)$ gives $W_z(t,f) = \delta(t-t_0)$ and equation (4) for the calculation of the cross-terms. The WVD is thus

$$\begin{aligned} W_{z_2}(t,f) &= \delta(t-t_0) + \delta(t-t_1) + 2\Re\left\{\int_{-\infty}^{\infty} \delta\left(t+\tfrac{\tau}{2}-t_0\right)\delta\left(t-\tfrac{\tau}{2}-t_1\right) e^{-2i\pi f\tau} d\tau\right\} \\ &= \delta(t-t_0) + \delta(t-t_1) + 2\delta\left(t - \tfrac{t_0+t_1}{2}\right)\cos\left(2\pi f\tfrac{t_0+t_1}{2}\right). \end{aligned} \tag{26}$$

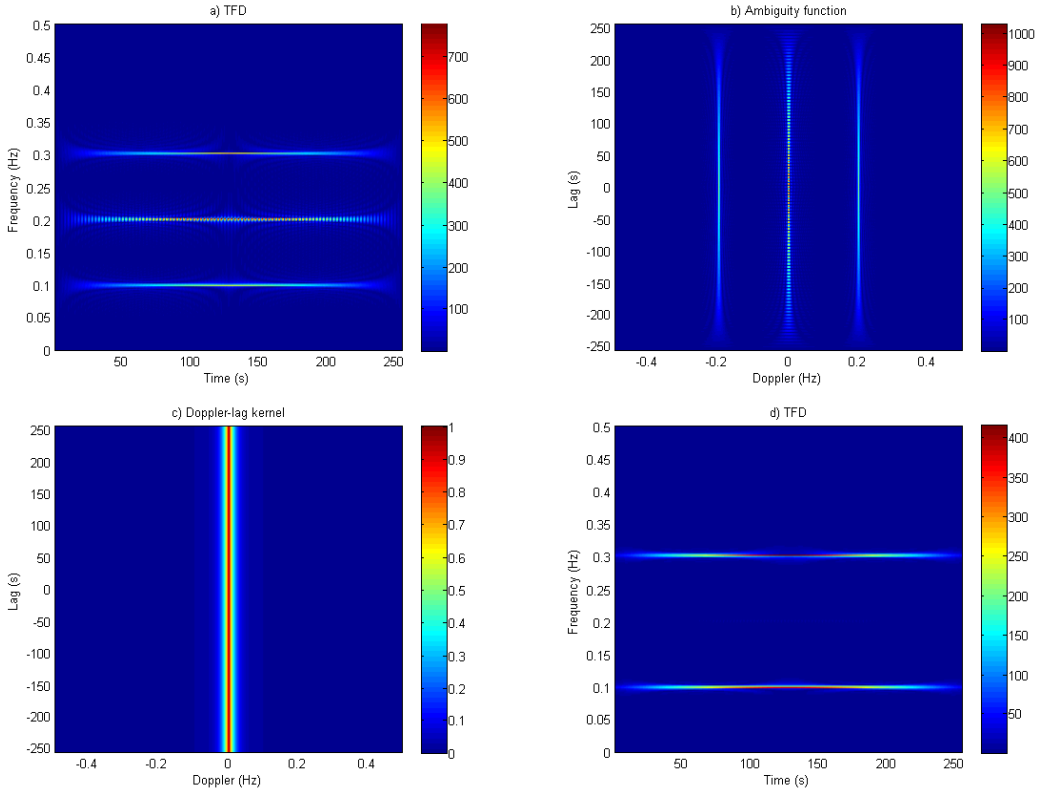

Figure 7: Time-frequency analysis related plots for the signal in equation (20) with $f_0 = 0.1$ and $f_1 = 0.3$. The signal duration is 256 seconds and the sampling frequency 2 Hz. a) The WVD of the signal. b) The ambiguity function of the signal. c) The LID kernel described in equation (23) with $\gamma = 75$. d) The filtered TFD of the signal using the LID kernel in c).

The WVD for a signal $z_2(t)$, with $t_0 = 80$ and $t_1 = 170$, is shown in Figure 8a). The figure clearly shows that the location of the auto- and cross-terms correspond to those given in the calculation above. The ambiguity function of the signal is

$$\begin{aligned} A_{z_2}(\nu,\tau) &= \int_{-\infty}^{\infty} \left(\delta\left(t+\tfrac{\tau}{2}-t_0\right)\delta\left(t+\tfrac{\tau}{2}-t_1\right)\right)\left(\delta\left(t-\tfrac{\tau}{2}-t_0\right)\delta\left(t-\tfrac{\tau}{2}-t_1\right)\right)^* e^{-i2\pi\nu t}dt \\ &= \int_{-\infty}^{\infty} \Big(\delta\left(t+\tfrac{\tau}{2}-t_0\right)\delta\left(t+\tfrac{\tau}{2}-t_0\right)+\delta\left(t-\tfrac{\tau}{2}-t_1\right)\delta\left(t-\tfrac{\tau}{2}-t_1\right) \\ &\qquad +\delta\left(t+\tfrac{\tau}{2}-t_0\right)\delta\left(t-\tfrac{\tau}{2}-t_1\right)+\delta\left(t+\tfrac{\tau}{2}-t_1\right)\delta\left(t-\tfrac{\tau}{2}-t_0\right)\Big)e^{-i2\pi\nu t}dt \\ &= \delta(\tau)\left(e^{i2\pi t_0\nu}+e^{i2\pi t_1\nu}\right)+\big(\delta(\tau-(t_0-t_1))+\delta(\tau+(t_0-t_1))\big)e^{i\pi(t_0+t_1)\nu}. \end{aligned} \tag{27}$$

This means that the auto-term will be located at $\tau = 0$ and the cross-terms at $\tau = \pm(t_0 - t_1)$ in the ambiguity domain. Figure 8b) shows this for the signal with $t_0 = 80$ and $t_1 = 170$, the cross-terms are indeed located at $\tau = \pm 90$. This ambiguity function can be multiplied with the same CD LID kernel as before, equation (23), which is shown in Figure 8c) with $\gamma = 25$. However the auto-terms will be suppressed due to the shape of the ambiguity function of the signal. In fact the auto- and cross-terms will be suppressed equally. The TFD resulting from filtering with

the LID kernel is complicated to calculate when multiplying $G_{\text{cd}}(\nu)$ with the ambiguity function, it is easier to calculate the convolution in time between WVD and the LID kernel. The LID kernel (23) in time domain is

$$g_{\text{cd}}(t) = \frac{\left(\gamma^2 + 4\pi^2 t^2\right)^{-1}}{\int_{-\infty}^{\infty} \left(\gamma^2 + 4\pi^2 \xi^2\right)^{-1} d\xi}, \tag{28}$$

as shown in [10]. The resulting TFD is then

$$\begin{aligned} \rho_{z_2}(t,f) &= g_{\text{cd}}(t) \underset{t}{*} W_{z_2}(t,f) \\ &= \frac{\left(\gamma^2 + 4\pi^2 (t-t_0)^2\right)^{-1} + \left(\gamma^2 + 4\pi^2 (t-t_1)^2\right)^{-1}}{\int_{-\infty}^{\infty} \left(\gamma^2 + 4\pi^2 \xi^2\right)^{-1} d\xi} \\ &+ \frac{2\left(\gamma^2 + 4\pi^2 \left(t - \frac{t_0+t_1}{2}\right)^2\right)^{-1} \cos\left(2\pi f \frac{t_0+t_1}{2}\right)}{\int_{-\infty}^{\infty} \left(\gamma^2 + 4\pi^2 \xi^2\right)^{-1} d\xi}. \end{aligned} \tag{29}$$

Full calculations are shown in Appendix B. It might be hard to imagine exactly how this will look, however it is clear that all auto- and cross-terms will be suppressed equally. It also possible to see that there will be smoothing in time, since the auto-terms no longer are delta functions, however the power will still be largest at $t = t_0$ and $t = t_1$. The filtered TFD of the signal (25) with $t_0 = 80$ and $t_1 = 170$, using the LID kernel with $\gamma = 25$ can be seen in Figure 8d). The smearing and suppression is evident.

It can be concluded that the LID kernel should perform well for slow varying FM signals, i.e. signals which have ambiguity functions where the auto-terms are close to $\nu = 0$. This thesis aims to analyse the performance of TFDs for such signals and will thus utilise LID kernels. The next sections, 5 and 6, will describe two methods which aim to further improve TFDs which uses LID kernels.

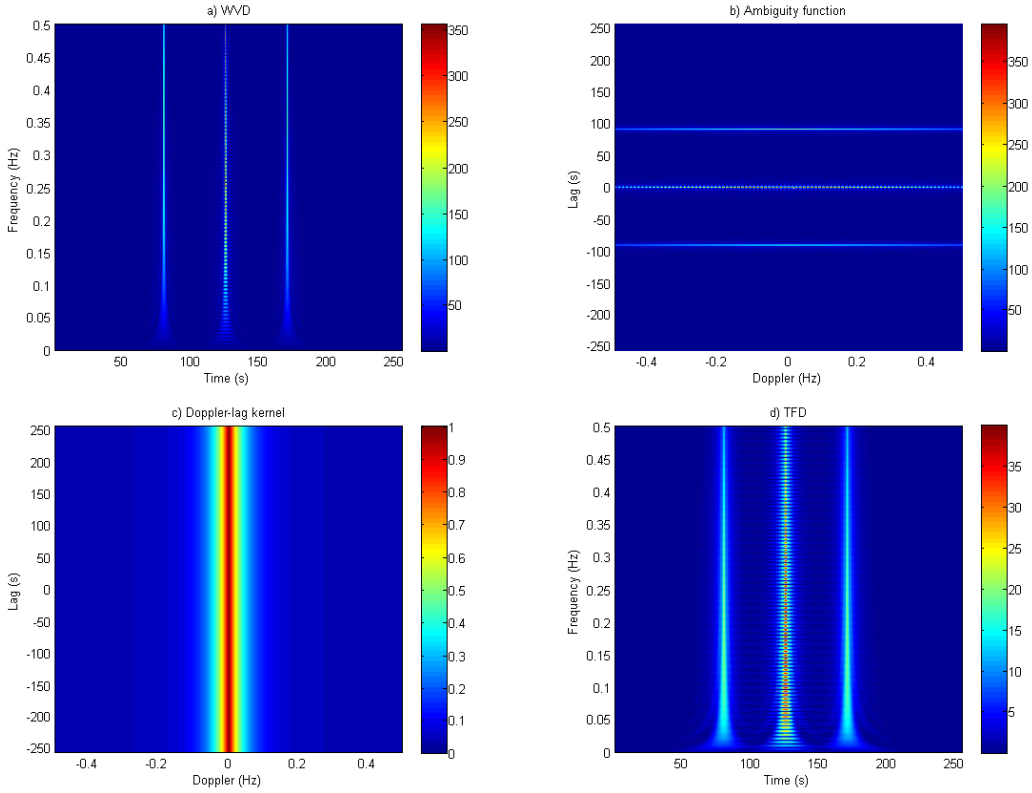

Figure 8: Time-frequency analysis related plots for the signal in equation (25) with $t_0 = 80$ and $t_1 = 170$. The signal duration is 256 seconds and the sampling frequency 2 Hz. a) The WVD of the signal. b) The ambiguity function of the signal. c) The LID kernel described in equation (23) with $\gamma = 25$. d) The filtered TFD of the signal using the LID kernel in c).

4 Performance measures

It is essential to have a measure for assessing the performance of TFDs. When looking at different TFDs it might be possible to say that some plots look cleaner and thus better. However assessing the performance based only on this visual comparison is very subjective, a more objective measurement is therefore required. This section will present two such measures.

The general guidelines, derived from the desired characteristics presented in Section 2.1, are that the signal components should be clearly resolved and the cross-terms should be suppressed. The auto-terms however should not be suppressed and any smoothing due to the filtering should be minimal.

4.1 Least normalised mean squared error

The WVD achieves the best energy concentration around the signal IF law and is considered to be optimal for (linear) mono-component signals. The sum of the WVDs of single components of a signal can therefore be considered the optimal performance of a TFD. This suggest that a

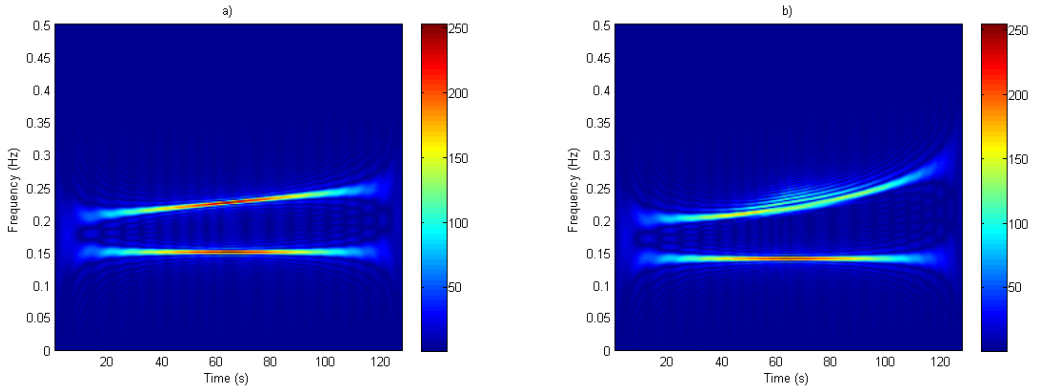

Figure 9: a) Sum of the WVDs for two mono-component linear FM signals. b) Sum of the WVDs for two mono-component FM signals, one linear and one non-linear.

performance measure can be defined using the normalised mean squared error (MSE)

$$P = 1 - \frac{\int_{-\infty}^{\infty}\int_{-\infty}^{\infty}\left(\rho_{\Sigma}(t,f) - \rho(t,f)\right)^2 df\,dt}{\int_{-\infty}^{\infty}\int_{-\infty}^{\infty}\rho_{\Sigma}(t,f)^2 df\,dt}, \quad P < 1, \tag{30}$$

where $\rho_{\Sigma}(t,f)$ is the sum of WVDs of the single components and $\rho(t,f)$ the TFD to be examined. A value close to 1 indicates a good performance. This performance measure has the following methodology

1. Divide the multi-component signal into its components and calculate the WVD for each of the signal components. Add the WVDs for the different signal components to get one WVD.

2. Normalise the obtained WVD and the TFD to be investigated so that the maximum absolute magnitude is 1.

3. Calculate the performance measure according to equation 30.

Note that the performance can be negative, it is negative when the compared TFD has more or wider components than the summarised WVD. This is due to the normalisation in step 2.

Figure 9a) shows the WVD obtained from summarising two mono-component linear FM signals, where one component increases linearly. This WVD clearly has good energy concentration around the components' IF laws. Figure 9b) shows the WVD obtained from summarising two mono-component FM signals, where one component is linear and the other increases non-linearly. In this plot the inner artifacts created by the non-linear component are clearly seen. The energy concentration is not optimal around the non-linear component's IF law. This suggest that this method of assessing the performance is not the best for non-linear FM signals.

4.2 Normalised instantaneous resolution performance measure

A good TFD has a high energy concentration about the IFs of each signal component and the components should be clearly resolved (see Section 2.1). A performance measure which combine these two concepts is presented by Boashash et al. in [14]. They call this the normalised instantaneous resolution performance measure and define it as

$$P(t) = 1 - \frac{1}{3}\left(\frac{A_S(t)}{A_M(t)} + \frac{1}{2}\frac{A_X(t)}{A_M(t)} + (1 - D(t))\right), \quad 0 < P(t) < 1, \tag{31}$$

where $A_S(t)$ is the average absolute amplitude of the largest sidelobes, $A_M(t)$ the average amplitude of the auto-terms (mainlobes), $A_X(t)$ the absolute amplitude of the cross-term and $D(t)$ a measure of the separation of the auto-terms. This performance measure is calculated for a time slice of the TFD, if $P(t)$ is calculated for several time slices t the average performance can be calculated. This method works well for signals with both linear and non-linear FM components [15], [16]. The only restriction is that the signal has two components.

Figure 10 shows two time slices of the TFDs of two different multi-component signals. In these the parameters of interest for calculating the performance measure are marked. The amplitudes of the signal components' mainlobes, A_{M1} and A_{M2}, are shown as the solid magenta lines. The average amplitude is thus the average of these.

The amplitudes of the largest sidelobes, A_{S1} and A_{S2}, are marked by the cyan lines. A sidelobe can be on the right or left side of the corresponding auto-term, compare Figures 10a) and 10b). The amplitude measurement A_S is always positive and is the average of the absolute values of A_{S1} and A_{S2}.

The amplitude of the cross-term is marked in green, A_X is the absolute value of the cross-term amplitude. The cross-term is the highest peak (or most negative peak) in the middle of the auto-terms. The cross-term can be the highest peak in the slice, see Figure 10b) which is a WVD, or much smaller compared with the auto-terms, see Figure 10a) which is a filtered TFD.

The parameter D is a measure of the separation of the signal components' mainlobes. It is defined as

$$D = \frac{\left(f_2 - \frac{V_2}{2}\right) - \left(f_1 - \frac{V_1}{2}\right)}{f_2 - f_1} = 1 - \frac{V}{\Delta f}, \tag{32}$$

where f_1 and f_2 are the IFs of the auto-terms, i.e. the centre of the mainlobes, shown as the dotted magenta lines in Figure 10. V_1 and V_2 are the instantaneous bandwidths of the auto-terms, calculated at $\frac{\sqrt{2}}{2}$ of the height of the mainlobe. The instantaneous bandwidths are shown in Figure 10 as the horizontal magenta lines. V is then the average of V_1 and V_2 and Δf the difference $f_2 - f_1$. Note that the index 1 indicates the component with the lowest IF, this means that D is positive and more separation gives a larger D.

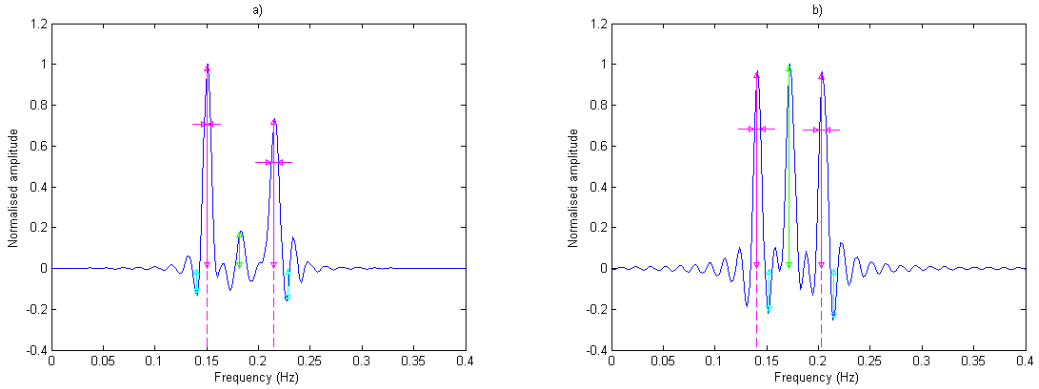

Figure 10: Time slices of the TFD of two different signals. The auto-terms (mainlobes) are marked by magenta, the dotted lines show their IFs and their instantaneous bandwidths are marked by the horizontal lines. The amplitudes of the auto-terms are shown with the solid magenta lines. The green line shows the amplitude of the cross-term. The cyan lines show the amplitudes of the sidelobes. a) The filtered TFD (CD kernel) of a two-component linear FM signal. b) The WVD of a two-component non-linear FM signal.

4.2.1 Method for automatic detection of auto- and cross-terms

In order to use the resolution performance measure there is a need for a method which automatically detects auto- and cross-terms for a time slice of a given TFD. The following method, also including the location of the largest sidelobes, is proposed by Sucic et al. in [15]

1. Normalise the time slice such that the absolute maximum is equal to 1.
2. Determine the three largest peaks of the slice.
3. Initially set the middle peak as the cross-term.
4. Check if the ratio of the amplitude of the remaining two peaks is close to 1 and if the peak chosen as cross-term is located between the other two peaks. If this is not true, choose the two largest peaks as auto-terms and the largest extremum (maximum or minimum) located in the middle of the auto-terms IFs as the cross-term.
5. The largest sidelobes are then located by finding first the largest outer extrema of the auto-terms (to the left of the first auto-term and to the right of the second) and then the largest inner extrema for each auto-term (between the auto-term and the cross-term). The largest of these extrema, around each auto-term, are the largest sidelobes.

This method is simple and does in many cases successfully identify the auto- and cross-terms. However there are unfortunately cases when it is unsuccessful, even when identification would seem simple. Figure 11a) shows an example where the three maximum peaks of a time slice are not in fact all the auto- and cross-terms. This could be solved by imposing a minimum distance on detected peaks or by identifying more than the three largest peaks.

One other problem with the method is that it relies on the amplitudes of the auto-terms being approximately equal. This is not always true and Figure 11b) shows such an example. Identifying the auto- and cross-terms in this slide might not be as easy as for Figure 11a), since this

is the WVD of a two-component FM signal with one non-linear component. The non-linearity of the second auto-term results in inner artifacts and a poorer energy concentration around the IF. The ratio between the amplitudes of the actual auto-terms is 1.56. This miss-identification will give a too large performance measure, since the estimated cross-term, marked with green, has much lower amplitude.

Suppose that the two outer peaks are identified as auto-terms and the peak in between them is sufficiently close to being located in the middle of them, then there might still exist another (minimum) extrema with larger absolute amplitude, sufficiently close to being located in the middle of the auto-terms. Figure 11c) shows an example of this, the peak marked with a green circle is the cross-term detected by the method. However the largest absolute amplitude of the cross-term is a negative peak, marked by a green asterisk. In the figure, the difference in normalised amplitude is 0.12 and the maximum deviation from the middle of the auto-terms is 4 samples. The difference in amplitudes might not seem much, but it will affect the performance measure. This problem is easily solved by always doing an additional search for the cross-term.

The proposed method struggles especially with identifying auto- and cross-terms for non-linear FM signals, due to the difference in amplitude of the two auto-terms. Since non-linear FM signals will be examined in this thesis it is essential to have a reliable method of detecting auto- and cross-terms in TFDs of these signals. The limitations of the method are also pointed out in [16] and the proposed solution involves an initial optimisation of the TFD, since the method performs better on filtered TFDs. This however means that the performance can not be measured for all WVDs or all TFDs filtered with wide kernels, whose performances are also interesting to now. The next section proposes a method which can measure the performance of such TFDs.

4.2.2 Improved method for automatic detection of auto- and cross-terms

With a few changes the method in the previous section can correctly identify the auto-terms, the cross-term and largest sidelobes. This improved method follows these steps

1. Normalise the time slice such that the absolute maximum is equal to 1.
2. Set a tolerance in samples for how much the cross-term can deviate from the middle of the auto-terms.
3. Determine a minimum (frequency) distance allowed between peaks when identifying the auto-terms. This distance should be a quarter of the bandwidth, in samples, of where all the positive peaks above some threshold amplitude are located. It should also be at least twice the tolerance, to allow for search of sidelobes between the auto-terms and the cross-term.
4. Identify the largest (positive) peaks, with minimum normalised amplitude 0.40, which are separated with at least the minimum distance. If at least two such peaks are identified, set the first as the first auto-term and the last as the last auto-term. Otherwise find the two largest peaks, separated by at least the minimum distance. If the amplitude of any of these peaks is less than the threshold amplitude used in the previous step set the performance measure to 0, otherwise set the first peak as the first auto-term and the other as the second.
5. **Optional** This step is used for measured signals. Check if the distance between the located auto-terms is smaller than some factor of the estimated bandwidth in step 3. If the distance is smaller, set the performance measure to 0.

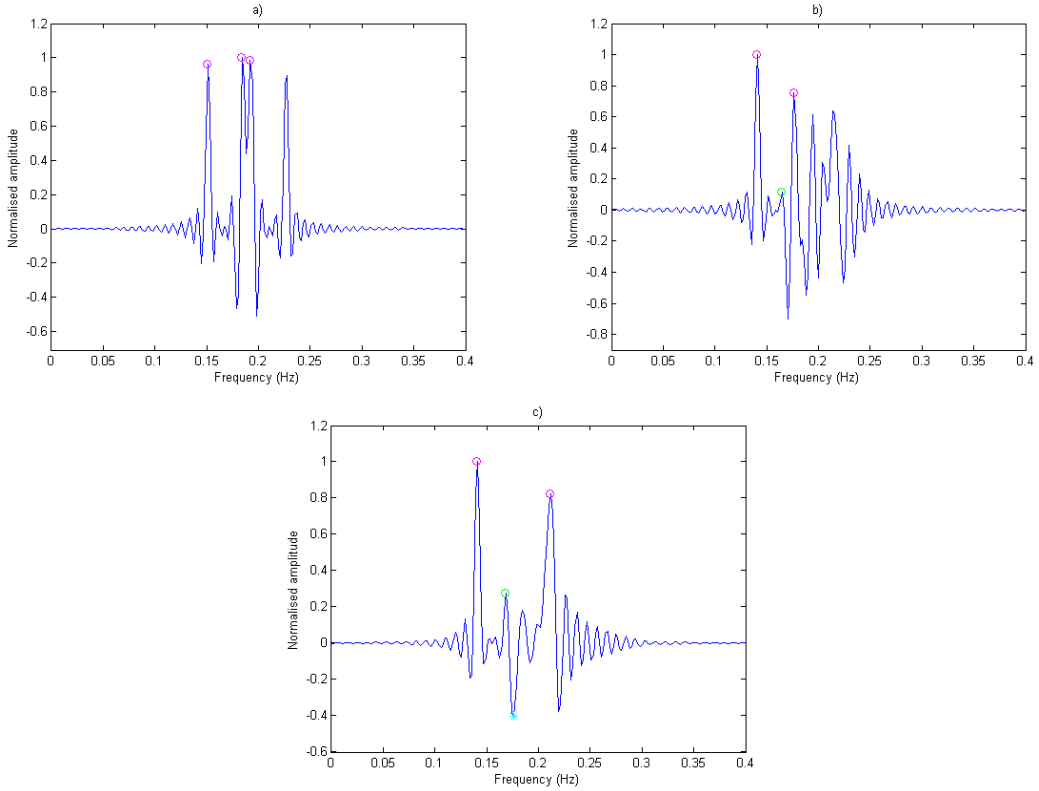

Figure 11: Time slices of different TFDs. a) WVD of a two-component linear FM signal. Largest three peaks are marked with magenta circles. b) WVD of a two-component non-linear FM signal. The peaks marked with magenta are the estimated auto-terms and the peak marked with green is the estimated cross-term. c) Filtered TFD of a two-component non-linear FM signal. The auto-terms are marked by magenta circles, the third largest (positive) peak, estimated cross-term, is marked by a green circle and the peak with maximum absolute amplitude in the middle of the auto-terms, actual cross-term, is marked by a cyan asterisk.

6. Find the extremum with the largest positive or negative amplitude in the middle of the auto-terms.

7. The largest sidelobes are then located by the same method as before.

The tolerance set in step 2 should ideally be rather small, but must allow for some uncertainty in the location of the peaks due to the signal being discrete. A tolerance equal to 4 samples has rendered good results. The threshold for the amplitudes in step 3 should ideally be large enough to not include any sidelobes but small enough to include both auto-terms. It could hence be set depending on the signal, good results have during testing with linear FM signals been obtained for a threshold around 0.15-0.20 (normalised amplitude). The reason for originally ignoring peaks which have normalised amplitude under 0.40 in step 4 is that the cross-term could be twice as large as the auto-terms for the WVD.

The optional step assures that one of the estimated auto-terms is not the cross-term. It is only used for measured signals because the step is not needed for simulated two-component signals and because the estimated bandwidth in step 3 is sometimes too large for the WVD of simulated signals, due to strong sidelobes. The estimated bandwidth is at least the frequency distance between the two auto-terms, therefore a minimum distance of 0.60 of the estimated bandwidth has been used in this thesis.

This method relies less on the amplitude of the auto-terms being approximately equal. Instead it assumes that the outer sidelobes, further than the minimum peak distance away from the auto-terms, have rather small normalised amplitudes. This assumption works very well for the TFDs of the linear and non-linear FM signals which are examined in this thesis.

Figure 12a) shows the time slice of the same WVD as in Figure 11a), and it can be seen that the improved method correctly identifies the auto-terms. The previous method results in a crash of the program since the distance between the largest two peaks is too small, the improved method gives a performance measure of $P(t_a) = 0.54$, where $t_a = 128$ is the time slice. The improved method also correctly identifies the auto-terms in the time slice shown in Figure 12b) (compare with Figure 11b)). The original method gives a performance measure $P_o(t_b) = 0.77$ and the improved method $P(t_b) = 0.55$, $t_b = 120$. Also for the time slice shown in Figure 11c) the improved method correctly identifies the auto- and cross-terms, see the result in Figure 12c). The original method gives $P_o(t_c) = 0.81$ and the new $P(t_c) = 0.78$, $t_c = 107$. The plots also show the bandwidth with the largest peaks for the time slices, this is marked by the black dashed lines.

It can be concluded that there is a difference in the calculated performance measure between the two methods. The improved method performs better on the TFDs and signals relevant to this thesis without the method being too signal dependent. The improved method will therefore be used when the performance of different TFDs are evaluated in Section 7.

4.3 Advantages and disadvantages of the two performance measures

Two different performance measures have been presented, they measure the performance in different ways and will thus give different optimal TFDs. The reasons for describing and using both are that they have different advantages and limitations. It will also demonstrate the importance of the choise of performance measure.

The method which uses the normalised MSE is easy to implement and will never fail to determine a measure for the performance. It also works for signals containing more than two components. The resolution measure is much harder to implement and could fail to identify the correct auto-terms which gives the wrong performance measure. This problem will also not be detected if not the identification of auto-terms is checked for each time slice. Also it can only measure the performance of two-component signals. However the normalised MSE only works on linear signals. In theory the resolution measure can be implemented on any signal with some modifications.

Another advantage with the proposed resolution measure is that it could be used on TFDs for measured signals. That is not possible for the normalised MSE method, since the signal components need to be known. Also worth mentioning is that even though the WVD is optimal for linear mono-component signals, there still are small ripples in the TFD. If an examined TFD has suppressed those ripples, the MSE will increase since the examined TFD differs form the optimal one. This is of course a disadvantage of the normalised MSE method.

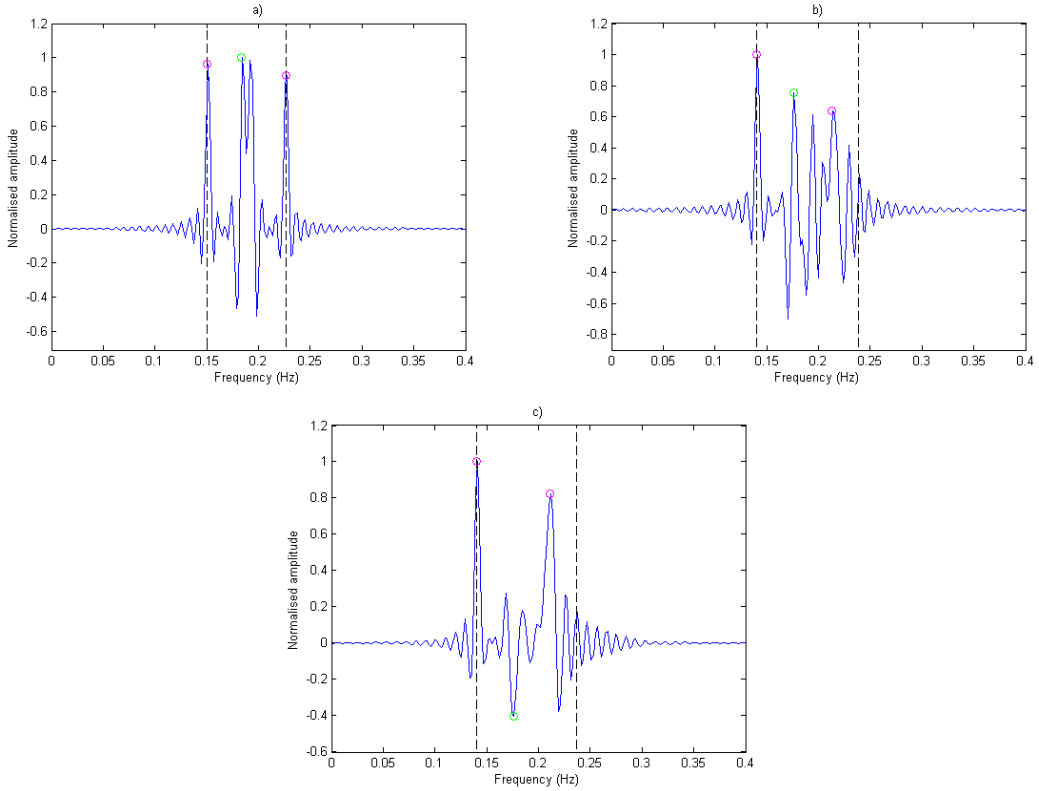

Figure 12: Time slices of different TFDs. a) WVD of a two-component linear FM signal, same as in Figure 11a). b) WVD of a two-component non-linear FM signal, same as in Figure 11b). c) Filtered TFD of a two-component linear FM signal, same as in Figure 11c). In all figures the magenta circles mark the auto-terms and the green the cross-term, the black dashed lines mark the bandwidth with the largest peaks.

5 Doppler restriction imposed on LID kernels

A new way of designing data-adaptive LID kernels to improve IF estimates of slow varying FM signals is proposed by Dong et al. in [10]. They propose a way to further reduce cross-terms and still keep resolution of auto-terms by imposing a Doppler restriction on LID kernels. In general a narrower LID kernel in the ambiguity domain results in more effective cross-term suppression, however the result is also poorer resolution of the auto-terms. The Doppler restriction is implemented by introducing a new variable ν_0 and let the kernel be zero for all $|\nu| \geq \nu_0$. This variable then acts like a cut-off frequency for the kernel in the ambiguity domain. This restriction can be applied for example to a modified B-distribution (MBD) kernel and a LID kernel based on the CD. These kernels have compact support (CS) and are therefore notated as CS-MBD and CS-CD. The Doppler CS-MBD kernel is

$$G_{\text{csmbd}}(\nu) = \begin{cases} \frac{|\Gamma(\beta+i\pi\nu)^2|}{\Gamma^2(\beta)}, & \text{if } |\nu| < \nu_0 \\ 0, & \text{otherwise,} \end{cases} \tag{33}$$

and the Doppler CS-CD is

$$G_{\text{cscd}}(\nu) = \begin{cases} e^{-\gamma|\nu|}, & \text{if } |\nu| < \nu_0 \\ 0, & \text{otherwise.} \end{cases} \tag{34}$$

In the article [10] this method is only tested on linear FM signals. In this thesis it will however also be tested on a non-linear FM signal. This gives two new problems, the non-linearity will result in inner artifacts, which the LID kernel will not be able to suppress. It will also mean that the signal will vary faster with time compared to the previously tested linear FM signals.

5.1 Selection of Doppler restriction

The suggested choice of Doppler restriction by Dong et al. [10] is $\nu_0 = \min|(f_p - f_q)|,\ p, q = 1, \ldots, P,\ p \neq q$ where f_p and f_q are frequencies of different signal components and P is the number of signal components. This is supported by the locations of cross-terms in the ambiguity domain for slowly varying FM signals. In the ambiguity domain the Doppler distance between auto- and cross-terms will be equal to the frequency distance between the signal components in the time-frequency domain, thus supporting the choice of ν_0 as minimum frequency distance between two signal components. This choice will however be examined by calculating the filtered TFD of the two-component signal (20) using a compact support kernel.

5.1.1 Different choices of Doppler restriction for the CS-CD kernel

The ambiguity function of the signal $z_1(t) = e^{i2\pi f_0 t} + e^{i2\pi f_1 t}$ was calculated in Section 3.3.2 and is

$$A_{z_1}(\nu, \tau) = \delta(\nu)\left(e^{i2\pi f_0 \tau} + e^{i2\pi f_1 \tau}\right) + \big(\delta(\nu + (f_0 - f_1)) + \delta(\nu - (f_0 - f_1))\big)e^{i\pi(f_0+f_1)\tau}. \tag{35}$$

Multiplication with the CS-CD kernel (34) gives

$$\begin{aligned} G_{\text{cscd}}(\nu)A_{z_1}(\nu, \tau) = \delta(\nu)e^{-\gamma|\nu|}&\left(e^{i2\pi f_o \tau} + e^{-2\pi f_1 \tau}\right) \\ &+ \Big(\delta(\nu + f_0 - f_1) + \delta(\nu - f_0 + f_1)\Big)e^{-\gamma|\nu|}e^{i\pi(f_0+f_1)\tau}, \quad \text{if } |\nu| < \nu_0, \end{aligned} \tag{36}$$

and 0 otherwise. This means that when calculating the TFD the auto- and cross-terms can be treated separately and the integration over ν and τ can be made separately.

Beginning with the integration over ν for the auto-term in equation 36, excluding the terms $e^{i2\pi f_o \tau}$ and $e^{-2\pi f_1 \tau}$ which depend on τ, the following is obtained

$$\int_{-\nu_0}^{\nu_0} \delta(\nu)e^{-\gamma|\nu|}e^{i2\pi t\nu}d\nu = 1. \tag{37}$$

Calculation for one of the cross-terms gives

$$\begin{aligned} &\int_{-\nu_0}^{\nu_0} \delta(\nu + f_0 - f_1)e^{-\gamma|\nu|}e^{i2\pi t\nu}d\nu \\ &= e^{-\gamma|f_0 - f_1|}e^{-i2\pi(f_0 - f_1)t}\theta(\nu_0 - |f_0 - f_1|), \end{aligned} \tag{38}$$

i.e. the integral takes the value $e^{-\gamma|f_0 - f_1|}e^{-i2\pi(f_0 - f_1)}$ if $\nu_0 > |f_0 - f_1|$. The integration for the other cross-term is calculated similarly

$$\begin{aligned} &\int_{-\nu_0}^{\nu_0} \delta(\nu - f_0 + f_1)e^{-\gamma|\nu|}e^{i2\pi t\nu}d\nu \\ &= e^{-\gamma|f_0 - f_1|}e^{i2\pi(f_0 - f_1)t}\theta(\nu_0 - |f_0 - f_1|). \end{aligned} \tag{39}$$

The integration over τ yields the same calculations as in Appendix A and the results are

$$\int_{-\infty}^{\infty} e^{i2\pi f_0\tau} e^{-i2\pi f\tau} d\tau = \delta(f - f_0), \tag{40}$$

$$\int_{-\infty}^{\infty} e^{i2\pi f_1\tau} e^{-i2\pi f\tau} d\tau = \delta(f - f_1), \tag{41}$$

and

$$\int_{-\infty}^{\infty} e^{i\pi(f_0+f_1)\tau} e^{-i2\pi f\tau} d\tau = \delta\left(f - \tfrac{f_0+f_1}{2}\right). \tag{42}$$

These calculations give

$$\begin{aligned}
\rho_{z_1}(t,f) &= \int_{-\infty}^{\infty}\int_{-\infty}^{\infty} G_{\text{cscd}}(\nu) A_{z_1}(\nu,\tau) e^{-i2\pi(\tau f - \nu t)} d\tau d\nu \\
&= \delta(f - f_0) + \delta(f - f_1) \\
&+ \delta\left(f - \tfrac{f_0+f_1}{2}\right) e^{-\gamma|f_0 - f_1|} \left(e^{i2\pi(f_0-f_1)t} + e^{-i2\pi(f_0-f_1)t}\right) \theta(\nu_0 - |f_0 - f_1|) \\
&= \delta(f - f_0) + \delta(f - f_1) \\
&+ 2\delta\left(f - \tfrac{f_0+f_1}{2}\right) e^{-\gamma|f_0 - f_1|} \cos(2\pi(f_0 - f_1)t) \theta(\nu_0 - |f_0 - f_1|).
\end{aligned} \tag{43}$$

It is now possible to consider the three cases $\nu_0 > |f_0 - f_1|$, $\nu_0 = |f_0 - f_1|$ and $\nu_0 < |f_0 - f_1|$.

Lets start with $\nu_0 > |f_0 - f_1|$. This gives the Heaviside function $\theta(\nu_0 - |f_0 - f_1|) = 1$ and the following TFD

$$\rho_{z_1}(t,f) = \delta(f - f_0) + \delta(f - f_1) + 2\delta\left(f - \tfrac{f_0+f_1}{2}\right) e^{-\gamma|f_0 - f_1|} \cos(2\pi(f_0 - f_1)), \tag{44}$$

which is the same filtered TFD as is obtained when no Doppler restriction exists, compare with (24) in Section 3.3.2. With this result it can be concluded that $\nu_0 > |f_0 - f_1|$ is not a good choice.

When $\nu_0 = |f_0 - f_1|$, the Heaviside function is $\theta(\nu_0 - |f_0 - f_1|) = \theta(0)$, which is a discontinuous point of the function. The approximation $\theta(0) = 1/2$ is often used and this gives

$$\rho_{z_1}(t,f) = \delta(f - f_0) + \delta(f - f_1) + \delta\left(f - \tfrac{f_0+f_1}{2}\right) e^{-\gamma|f_0 - f_1|} \cos(2\pi(f_0 - f_1)). \tag{45}$$

The cross-term is now suppressed by an additional factor 2 compared to when using no Doppler restriction.

Finally lets consider the case $\nu_0 < |f_0 - f_1|$. The Heaviside function is then $\theta(\nu_0 - |f_0 - f_1|) = 0$ and the cross-term is fully suppressed giving the following filtered TFD

$$\rho_{z_1}(t,f) = \delta(f - f_0) + \delta(f - f_1). \tag{46}$$

Only the two delta functions, representing the two signal components, are left. Given this result $\nu_0 < |f_0 - f_1|$ would seem the optimal choice for the Doppler restriction. However if examining the used LID kernel again, it can be noted that it is defined to be zero when $|\nu| \geq \nu_0$, nevertheless when calculating the filtered TFD the integral boundaries for ν are $\pm\nu_0$. This is of course correct in the continuous and infinite case. In applications however the signals and their representations in different domains are discrete. Since the CS-CD kernel will be 0 on the actual

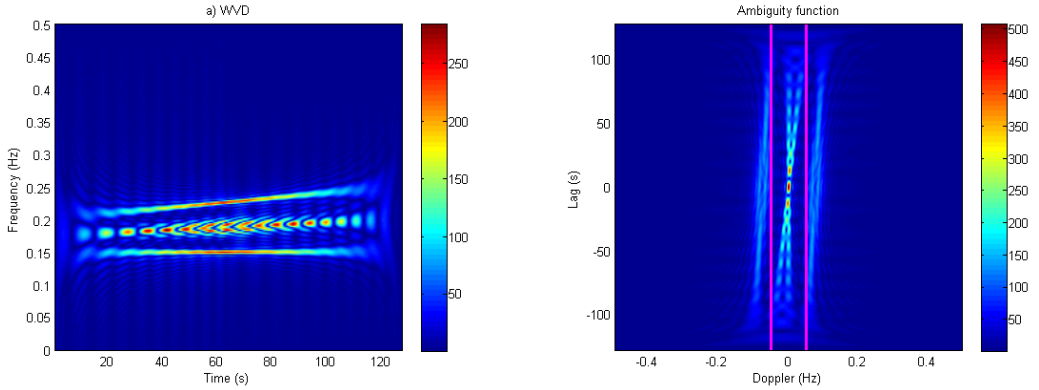

Figure 13: WVD and ambiguity function for a signal with a slow moving linear FM component. a) The WVD of the signal. b) The ambiguity function of the signal with the magenta lines representing $\nu = \pm 0.05$ Hz, the minimum frequency distance of the frequency components. The signal duration is 128 seconds and the sampling frequency 2 Hz.

samples representing $\nu = \pm\nu_0$, the Doppler restriction can be chosen as $\nu_0 = |f_0 - f_1|$ to suppress both cross-terms completely.

It is preferred to choose the Doppler restriction as large as possible while still suppressing any cross-terms. For the signal used in the calculations above an optimal choice of Doppler restriction would be any $\nu_0 \leq |f_0 - f_1|$ since the auto-terms are located at $\nu = 0$. This is if course often not the case for real signals. Figure 13 shows the WVD and ambiguity function of a signal with a slow moving linear FM component. In Figure 13b) the minimum frequency distance between the two signal components is marked ($\nu = \pm 0.05$ Hz) and it can clearly be seen that choosing this as the Doppler restriction will suppress most of the cross-terms and still keep much of the auto-terms. If ν_0 would be set smaller than the minimum frequency distance this would further suppress the auto-terms which will cause smearing of the auto-terms in the time-frequency domain.

When considering application to measured signals, the minimum frequency distance might not always be known. To be able to determine the Doppler restriction the minimum frequency distance of the signal first needs to be estimated. To do this for example a periodogram, spectrum or spectrogram can be calculated.

6 Multitaper TFDs with limited Doppler bandwidth

The concept of multitaper was presented in [11] and it proposes the use of several tapers (windows) to estimate the spectra of a stationary process. This concept has been expanded to produce the multitaper spectrogram. The advantage with the multitaper spectrogram is that strong sidelobe suppression can be achieved and that it is computationally effective. Using the relationship between the spectrogram and the WVD described in Section 2.5 and expanding to a multitaper spectrogram, a computationally effective way of calculating a filtered TFD is found. The method uses that any quadratic TFD can be decomposed into a weighted sum of spectrograms [7]. When calculating a filtered TFD with this method, the eigenvalues and eigenvectors of the rotated time-lag kernel are used. The filtered TFD is the weighted sum of the spectrograms of

the signal with the different eigenvectors as sliding windows and the eigenvalues as weights [12]. The multitaper spectrogram is defined as

$$S_z(t,f) = \sum_{k=1}^{K} \alpha_k \left| \int_{-\infty}^{\infty} z(t_1) h_k^*(t-t_1) e^{-i2\pi f t_1} dt_1 \right|^2, \tag{47}$$

where $z(t)$ is the signal (in this case analytic), α_k the weights and $h_k(t)$ the taper functions. Section 2.5 showed that the spectrogram could be written as

$$\rho_z(t,f) = \int_{-\infty}^{\infty} G(t,\tau) \underset{t}{*} K_z(t,\tau) e^{-i2\pi f \tau} d\tau, \tag{48}$$

with $G(t,\tau) = h(t+\frac{\tau}{2})h^*(t-\frac{\tau}{2})$. The time-lag kernel for the multitaper spectrogram is then

$$G(t,\tau) = \sum_{k=1}^{K} \alpha_k h_k\left(t+\tfrac{\tau}{2}\right) h_k^*\left(t-\tfrac{\tau}{2}\right). \tag{49}$$

The rotated time-lag kernel is

$$G^{\mathrm{rot}}(t_1,t_2) = G\left(\tfrac{t_1+t_2}{2}, t_1-t_2\right). \tag{50}$$

Assuming that the rotated time-lag kernel satisfies the Hermitian property, the eigenvalues λ_k and eigenvectors $q_k(t)$ are obtained from solving

$$\int G^{\mathrm{rot}}(t_1,t_2) q(t_1) dt_1 = \lambda q(t_2). \tag{51}$$

The eigenvalues are then used as weights α_k and the eigenvectors as tapers $h_k(t)$ [13].

6.1 Cross-term suppression with limited Doppler bandwidth

In the article [13] by Hansson-Sandsten, the multitapers corresponding to the Wigner and Choi-Williams [7], [8] distributions are used together with penalty functions to suppress cross-terms outside a Doppler-lag bandwidth. The presented penalty function can suppress both outside a Doppler bandwidth and a lag bandwidth. For the purpose of this thesis only suppression outside a Doppler bandwidth is relevant. The multitapers used in this thesis will not be ones corresponding to Wigner and Choi-Williams distributions, but instead CD and MBD, which work better with FM signals. The signals tested in the article are not FM signals, but instead other multi-component signals. The hope is that this method will be successful in resolving linear and non-linear FM signals as well.

In accordance with [13] the modified penalty function is defined as

$$W_\nu(t_1,t_2) = P\delta(t_1-t_2) - (P-1)\Delta\nu_p \mathrm{sinc}(\Delta\nu_p(t_1-t_2)), \tag{52}$$

where $\mathrm{sinc}(x) = \frac{\sin(\pi x)}{\pi x}$. The penalty function is given in rotated time-lag domain. This penalty function thus suppresses with a factor P outside a predetermined interval $\Delta\nu_p$. This results in suppression outside a frequency distance of $\frac{\Delta\nu_p}{2}$ from every auto-term in the TFD. This is easily seen from the corresponding spectral density penalty function

$$S_P(f) = \begin{cases} P, & \text{if } |f| \geq \frac{\Delta\nu_p}{2}, \\ 1, & \text{otherwise.} \end{cases} \tag{53}$$

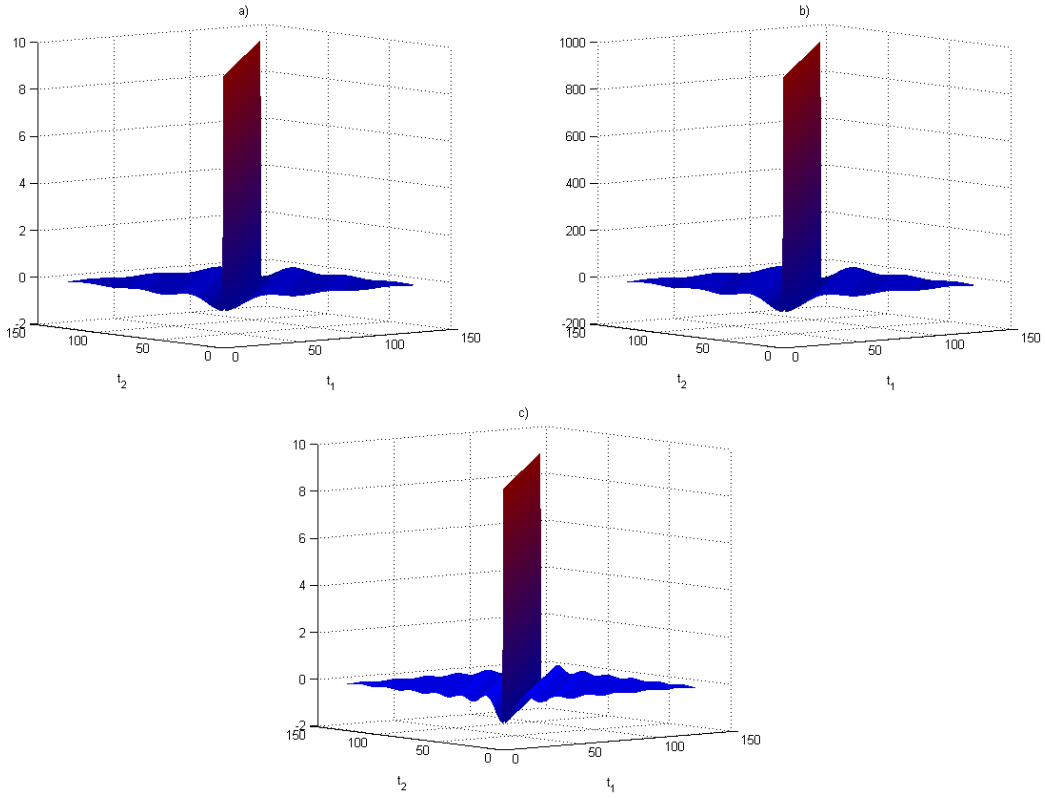

Figure 14: The penalty functions, rotated time-lag domain, for two different penalties and Doppler bandwidths. a) The penalty function with penalty $P = 10$ dB and Doppler bandwidth $\Delta\nu_p = 0.1$. b) The penalty function with penalty $P = 30$ dB and Doppler bandwidth $\Delta\nu_p = 0.1$. c) The penalty function with penalty $P = 10$ dB and Doppler bandwidth $\Delta\nu_p = 0.2$.

The tapers and weights using the penalty function are given by the solution to

$$\int G^{\text{rot}}(t_1, t_2)q(t_1)dt_1 = \lambda \int W_\nu(t_1, t_2)q(t_1)dt_1. \tag{54}$$

The penalty functions for two different penalty levels P and Doppler bandwidths $\Delta\nu_p$ are shown in Figure 14. Note that the penalty function is in time-lag domain and is rotated in this domian such that time is on the diagonal intercepting $t_1 = 0$, $t_2 = 0$ and $t_1 \to \infty$, $t_2 \to \infty$. An increased penalty level results in a penalty function with higher amplitude, compare Figures 14a) with $P = 10$ dB and 14b) with $P = 30$ dB. This gives stronger suppression outside the Doppler bandwidth. An increased Doppler bandwidth results in the sinusoidal waves having higher amplitudes and frequencies, compare Figure 14a) with $\Delta\nu_p = 0.1$ and Figure 14c) with $\Delta\nu_p = 0.2$. This means that less of the TFD is suppressed.

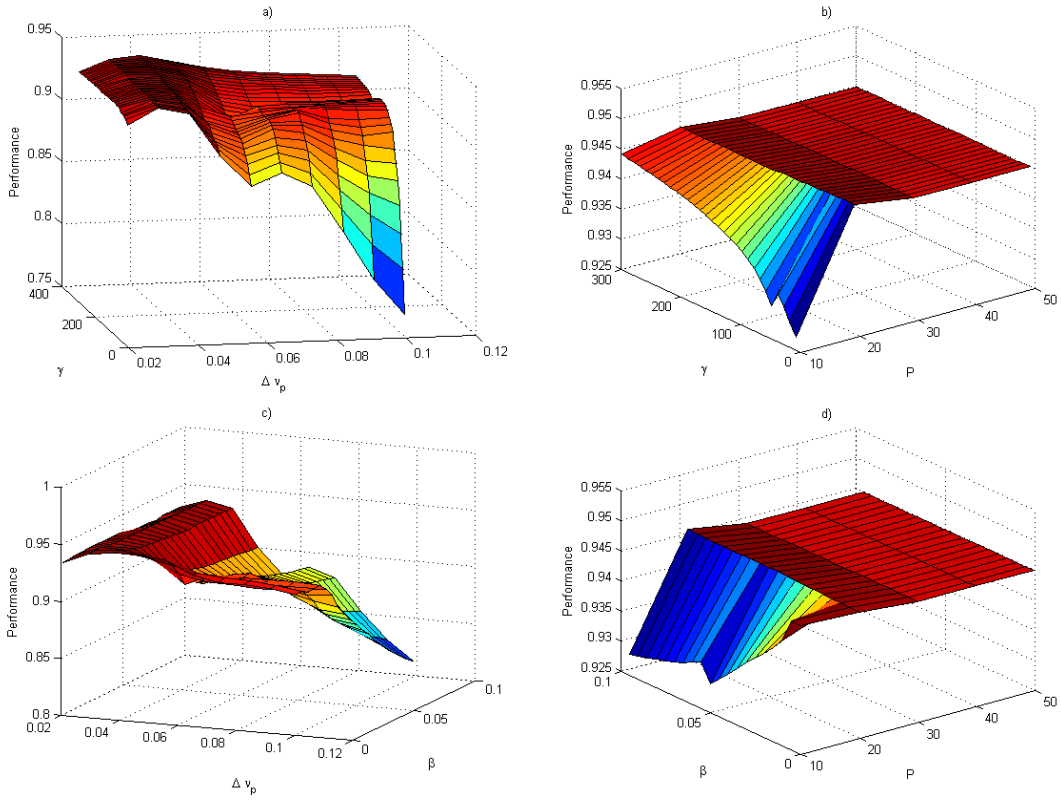

Figure 15: The effect on performance for different choices of Doppler bandwidth $\Delta\nu_p$ and suppression level P for the penalty function. Applied on two different kernels with varying scaling parameter. The signal used is a two-component linear FM signal. a) The performance measure of a multitaper TFD using a CD kernel for different scaling parameter γ and Doppler bandwidth $\Delta\nu_p$. b) The performance measure of a multitaper TFD using a CD kernel for different scaling parameter γ and suppression level P. c) The performance measure of a multitaper TFD using a MBD kernel for different scaling parameter β and Doppler bandwidth $\Delta\nu_p$. d) The performance measure of a multitaper TFD using a CD kernel for different scaling parameter β and suppression level P.

6.1.1 Choice of Doppler bandwidth and suppression level

The choice of Doppler bandwidth $\Delta\nu_p$ and suppression level P are signal and kernel dependent. The Doppler bandwidth is slightly related to the Doppler restriction of the CS LID kernel discussed in Section 5.1. The optimal Doppler restriction is the minimum frequency distance between signal components, the optimal Doppler bandwidth for a multitaper TFD is not as unambiguous. However it is reasonable to assume that the Doppler bandwidth should not be chosen larger than twice the minimum frequency distance. If it is, the cross-terms will not be suppressed. It could be chosen smaller than twice the minimum frequency distance since anything outside this bandwidth will be suppressed by a factor P and not removed entirely. Note that Figures 15a) and 15c) show how performance of a multitaper TFD can vary with different values of Doppler bandwidth. The smallest Doppler bandwidth examined is $\Delta\nu_p = 0.02$, so that auto-term will not be suppressed. The figures show that different Doppler bandwidth could give

optimal results, however for these two kernels, CD and MBD, and signal, the optimal choice seem to be much smaller than twice the minimum frequency distance ($|f_0 - f_1| = 0.05$).

Different levels of suppression can also be used to optimise the performance of a multitaper TFD. Figures 15b) and 15d) show the performance for suppression levels 10-50 dB, which seemed to be reasonable choices. From the figures it can be seen that best performance is obtained with suppression levels around 10-30 dB, if the suppression is increased beyond that no improvement is obtained. This result might only apply to the kernels and type of signal examined (CD and MBD on a two-component FM signal), however for the purpose of this thesis that is sufficient results.

7 Performance of different TFDs using CS LID kernels and multitaper with limited Doppler bandwidth

This section will examine the performance of the WVD, TFDs filtered with CD, CS-CD, MBD and CS-MBD kernels and multitaper TFDs using CD and MBD kernels, with and without suppression outside a limited Doppler bandwidth for two simulated FM signals. The FM signals are chosen because they closely resemble the measured HRV signals. If the methods of compact support kernels and multitapers with penalty functions show increased performance of their TFDs for the simulated FM signals, it suggests that the methods could yield improved TFDs for the HRV data.

The multitaper TFDs with suppression outside a limited Doppler bandwidth will be called LB (limited bandwidth) in figures and tables. Table 1 shows all the abbreviations for the different TFDs that will be assessed and which TFD they represent. The two performance measures, the normalised instantaneous resolution performance measure and the least normalised MSE performance measure, will be used to find the optimal TFD. The methodology used here for comparing the different TFDs is as follows

1. Divide the signal length with 6 and discard the first and last sixth of the TFD to be evaluated (time only). This removes the smeared part of the signal due to the edge effect.
2. If the signal is linear, calculate the MSE compared to the optimal WVD for the cut TFD.
3. Calculate the resolution performance for each time slice of the cut TFD, average this to obtain a performance measure for the whole TFD.
4. Optimise the TFD, i.e. the parameter for the distribution of the LID kernel, with regard to the performance measure or measures. If both performance measures are used this might result in two different TFDs.
5. Compare the performance measures of all the different TFDs. For linear FM signals the two different performance measures should be compared separately.

TFD abbreviation	Meaning
WVD	Wigner-Ville distribution
CD	TFD filtered with Cauchy distributed LID kernel
CS-CD	TFD filtered with compact support Cauchy distributed LID kernel
Multitaper CD	Multitaper TFD using Cauchy distributed LID kernel
Multitaper LB-CD	Multitaper TFD using Cauchy distributed LID kernel and suppression with penalty function
MBD	TFD filtered with modified B-distributed LID kernel
CS-MBD	TFD filtered with compact support modified B-distributed LID kernel
Multitaper MBD	Multitaper TFD using modified B-distributed LID kernel
Multitaper LB-MBD	Multitaper TFD using modified B-distributed LID kernel and suppression with penalty function

Table 1: Explanation of TFD abbreviations.

7.1 Simulated linear FM signal

In this section the performances for different TFDs of a two-component linear FM signal will be assessed. The signal components are close in frequency and the methods using CS kernels and multitapers with penalty functions aim to further resolve the components while keeping the energy concentration around the components' IF laws. The parameters and TFDs resulting from the optimisation according to the two performance measures, the normalised instantaneous resolution performance measure and the least normalised MSE performance measure, will be presented in two tables and a few figures. The simulated signal used is

$$s_l(t) = \cos(2\pi 0.15t) + \cos\left(2\pi\left(0.20t + \tfrac{0.05}{2\cdot 128}t^2\right)\right), \quad 0 \leq t \leq 128, \tag{55}$$

and the signal is sampled with 2 Hz. This is a real valued signal and the analytic signal is obtained using the Hilbert transform.

Table 2 shows the results of the optimisation when made with respect to the normalised instantaneous resolution performance measure. It shows the parameters for each TFD, the resolution measure and the corresponding least normalised MSE performance measure. According to the table, the multitaper TFDs with penalty functions are the best performing TFDs, these are shown in Figures 17d) and 18d). The advantage with these TFDs is that the cross-terms and sidelobes are completely suppressed, however there is loss in frequency resolution. Looking at the TFDs filtered with CS-CD and CS-MBD, Figures 17b) and 18b), they perform better than their non-compact counterpart kernels (Figures 17a) and 18a)). The CS-CD and CS-MBD TFDs get slightly lower performance than the multitaper TFDs because the kernel suppresses the second auto-term, however they have much less smearing in frequency compared to the multitaper TFDs. Figure 16 shows the WVD.

TFD	Optimal parameter(s)	Resolution measure	MSE measure
WVD	N/A	0.626	0.215
CD	$\gamma = 83$	0.919	0.765
CS-CD	$\gamma = 77$, $\nu_0 = 0.05$	0.920	0.779
Multitaper CD	$\gamma = 316$	0.929	-0.122
Multitaper LB-CD	$\gamma = 50$, $\Delta\nu_p = 0.038$, $P = 20$ dB	0.945	-1.625
MBD	$\beta = 0.036$	0.920	0.780
CS-MBD	$\beta = 0.037$, $\nu_0 = 0.05$	0.922	0.784
Multitaper MBD	$\beta = 0.009$	0.927	-0.090
Multitaper LB-MBD	$\beta = 0.058$, $\Delta\nu_p = 0.038$, $P = 20$ dB	0.945	-1.626

Table 2: Parameters and performance measure for different TFDs of the simulated signal in (55), optimised according to the normalised instantaneous resolution performance measure.

Table 3 shows the results of the optimisation when made with respect to the least normalised MSE performance measure. Figures 19 - 20 show the TFDs. According the MSE measure, the best TDF is the one filtered with the CS-MBD kernel, with CS-CD yielding almost as good performance. Figures 20b) and 19b) show these TFDs. The second auto-term is not as suppressed as in Figures 17b) and 18b), however more of the cross-term remain.

According to Table 3 the performance for the multitaper TFDs is very bad. The Figures 19c)-d) and 20c)-d) show the TFDs. The reason why these are performing bad according to the normalised MSE performance measure is the smearing in frequency, which will yield large MSE since the optimal WVD has no smearing in frequency, see Figure 9a).

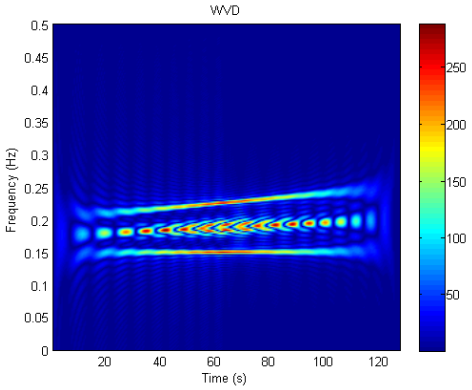

Figure 16: The WVD of the simulated signal in (55).

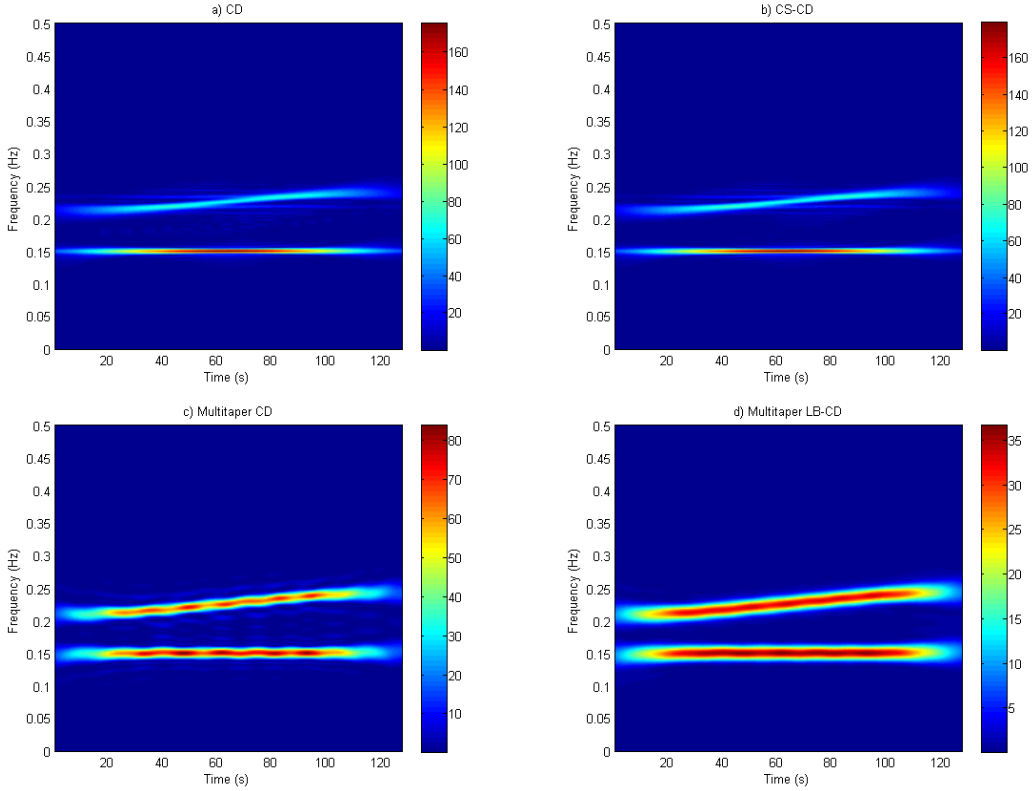

Figure 17: TFDs of the simulated signal in (55), using the CD kernel optimised with respect to the normalised instantaneous resolution performance measure. a) TFD filtered with CD kernel. b) TFD filtered with CS-CD kernel. c) Multitaper TFD using CD kernel. d) Multitaper TFD using LB-CD kernel.

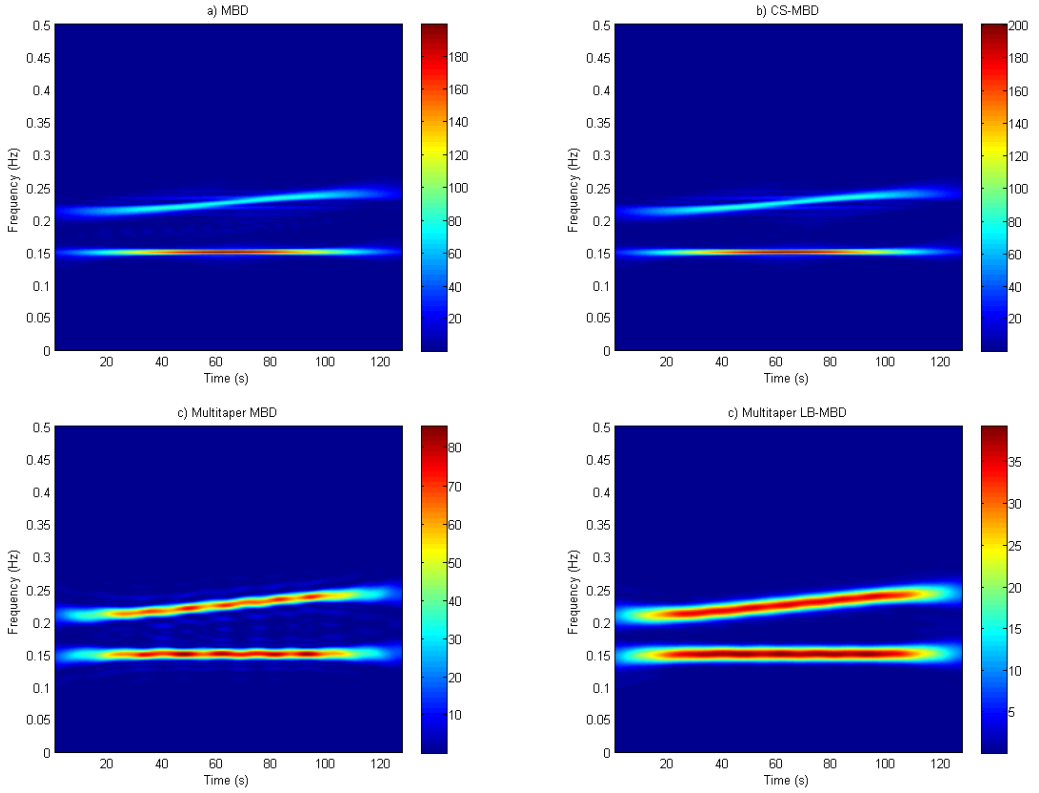

Figure 18: TFDs of the simulated signal in (55), using the MBD kernel optimised with respect to the normalised instantaneous resolution performance measure. a) TFD filtered with MBD kernel. b) TFD filtered with CS-MBD kernel. c) Multitaper TFD using MBD kernel. d) Multitaper TFD using LB-MBD kernel.

TFD	Optimal parameter(s)	MSE measure	Resolution measure
WVD	N/A	0.215	0.626
CD	$\gamma = 31$	0.872	0.878
CS-CD	$\gamma = 6$, $\nu_0 = 0.05$	0.931	0.882
Multitaper CD	$\gamma = 75$	0.046	0.887
Multitaper LB-CD	$\gamma = 0.1$, $\Delta\nu_p = 0.091$, $P = 10$ dB	0.196	0.763
MBD	$\beta = 0.098$	0.891	0.873
CS-MBD	$\beta = 0.221$, $\nu_0 = 0.05$	0.932	0.881
Multitaper MBD	$\beta = 0.036$	0.046	0.882
Multitaper LB-MBD	$\beta = 0.041$, $\Delta\nu_p = 0.100$, $P = 10$ dB	-0.355	0.882

Table 3: Parameters and performance measure for different TFDs of the simulated signal in (55), optimised according to the normalised MSE performance measure.

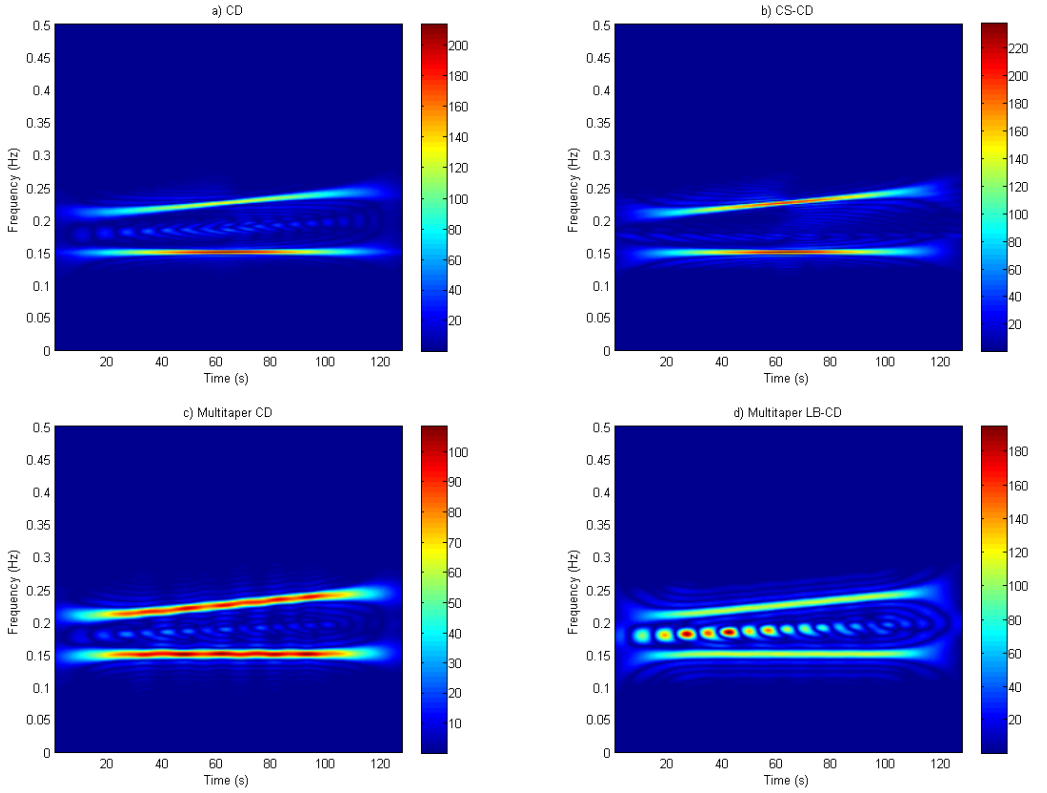

Figure 19: TFDs of the simulated signal in (55), using the CD kernel optimised with respect to the normalised least MSE performance measure. a) TFD filtered with CD kernel. b) TFD filtered with CS-CD kernel. c) Multitaper TFD using CD kernel. d) Multitaper TFD using LB-CD kernel.

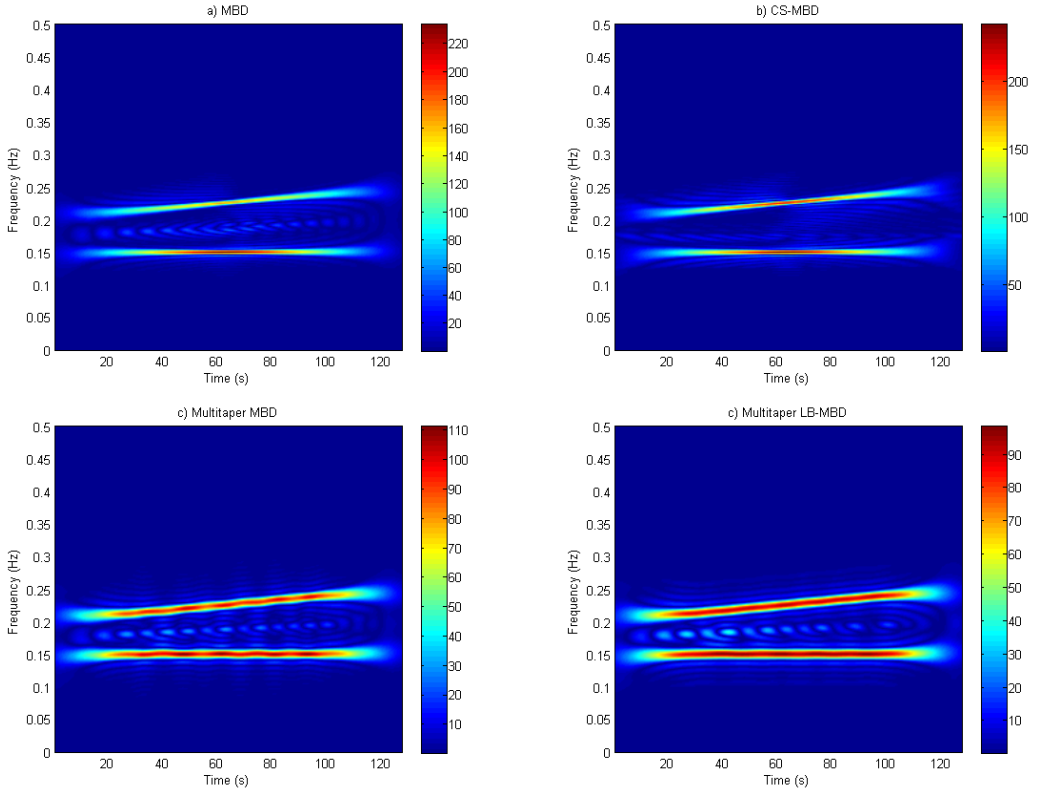

Figure 20: TFDs of the simulated signal in (55), using the MBD kernel optimised with respect to the normalised least MSE performance measure. a) TFD filtered with MBD kernel. b) TFD filtered with CS-MBD kernel. c) Multitaper TFD using MBD kernel. d) Multitaper TFD using LB-MBD kernel.

7.2 Simulated non-linear FM signal

In this section the performance for different TFDs of a two-component non-linear FM signal will be assessed. The parameters and TFDs resulting from the optimisation according to only the normalised instantaneous resolution performance measure will be presented in a tables and a few figures. The simulated signal used is

$$s_{nl}(t) = \cos(2\pi 0.14t) + \cos\left(2\pi\left(0.20t + \tfrac{0.1}{4\cdot 128^3}t^4\right)\right), \quad 0 \le t \le 128, \tag{56}$$

and the signal is sampled with 2 Hz. Note that this is a real valued signal and the analytic signal is obtained using the Hilbert transform.

According to Table 4 the best TDFs are the multitaper TFDs with CD and MBD kernels and suppression outside a Doppler bandwidth. Looking at the Figures 21 - 23 this result is also apparent. The non-multitaper TFDs suppress the second auto-term significantly, especially as it increases in frequency. The reason for this is of course that in the ambiguity function of the signal this auto-term deviates much from $\nu = 0$. Also the resolution performance measure will allow the LID kernel to become narrow enough to suppress the second auto-term in order to also suppress the inner artifacts created by this auto-term. With the definition of the normalised

TFD	Optimal parameter(s)	Resolution measure
WVD	N/A	0.609
CD	$\gamma = 74$	0.915
CS-CD	$\gamma = 69$, $\nu_0 = 0.06$	0.918
Multitaper CD	$\gamma = 249$	0.908
Multitaper LB-CD	$\gamma = 96$, $\Delta\nu_p = 0.053$, $P = 20$	0.939
MBD	$\beta = 0.036$	0.917
CS-MBD	$\beta = 0.040$, $\nu_0 = 0.06$	0.918
Multitaper MBD	$\beta = 0.002$	0.910
Multitaper LB-MBD	$\beta = 0.029$, $\Delta\nu_p = 0.053$, $P = 20$	0.939

Table 4: Parameters and performance measure for different TFDs of the simulated signal in (56), optimised according to the normalised resolution performance measure.

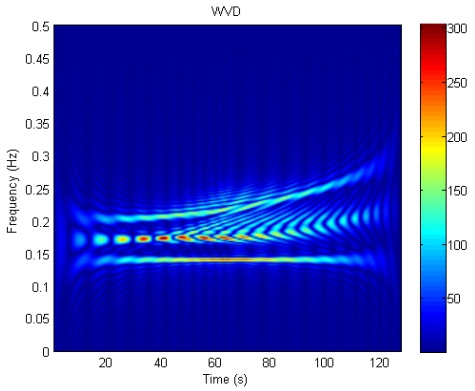

Figure 21: The WVD of the simulated signal in (56).

instantaneous resolution performance measure being as it is, this decrease in cross-term and sidelobe magnitudes will give an increased performance measure. The CS kernels still have better performance than the non-CS kernels, however not by much since the frequency distance between the components is not small for much of the signal duration.

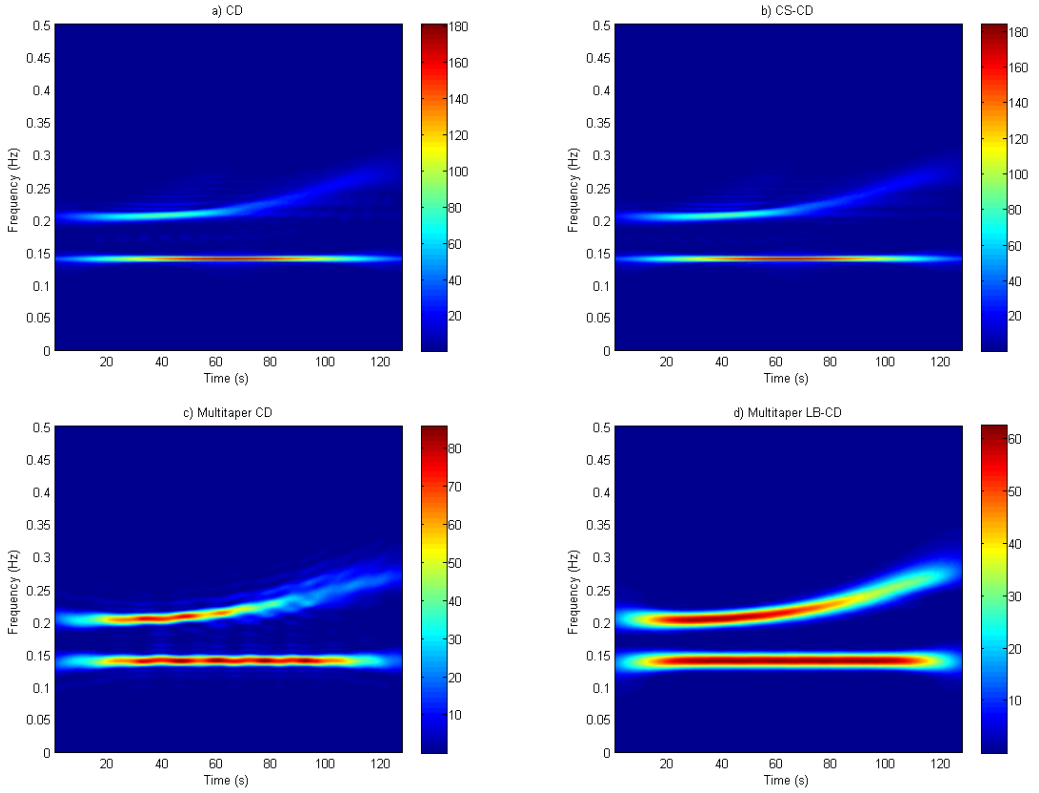

Figure 22: Optimal TFDs of the simulated signal in (56), using the CD kernel. a) TFD filtered with CD kernel. b) TFD filtered with CS-CD kernel. c) Multitaper TFD using CD kernel. d) Multitaper TFD using LB-CD kernel.

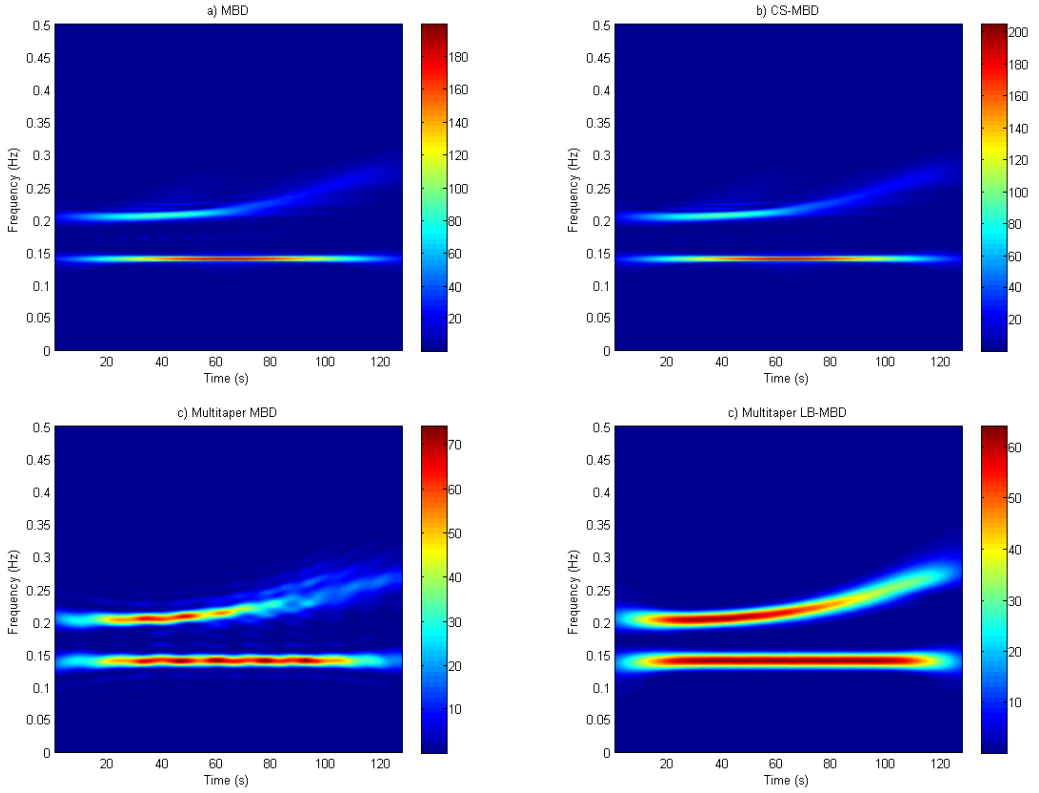

Figure 23: Optimal TFDs of the simulated signal in (56), using the MBD kernel. a) TFD filtered with MBD kernel. b) TFD filtered with CS-MBD kernel. c) Multitaper TFD using MBD kernel. d) Multitaper TFD using LB-MBD kernel.

7.2.1 Performance measure with higher threshold amplitude

In the last section it could be seen that optimisation using the normalised instantaneous resolution performance measure suppresses the second auto-term significantly. Though this might result in a high performance measure it might not be desirable. A small modification to the implemented method can be done however, penalising differences in the auto-term magnitudes more. This will yield other optimal TFDs. In this section only the TFDs obtained through simple filtering of the LID kernels, both CS and not, will be assessed, since the results for multitaper TFDs were good.

A larger penalty for large difference in auto-term amplitudes can be imposed by increasing the threshold amplitude discussed in the method, see Section 4.2.2. For all the previous optimisation it has been 0.15 (normalised amplitude), in this section it will be set to 0.30 instead. The direct result of this is that any time slice where the second (or first) auto-term has a normalised amplitude less than 0.30, the performance will be set to 0. This means that the performance measure will not increase for TFDs where the second auto-term is less suppressed, instead the maximum performance will decrease.

TFD	Optimal parameter(s)	Resolution measure
CD	$\gamma = 36$	0.884
CS-CD	$\gamma = 38$, $\nu_0 = 0.06$	0.903
MBD	$\beta = 0.073$	0.888
CS-MBD	$\beta = 0.070$, $\nu_0 = 0.06$	0.902

Table 5: Parameters and performance measure for different TFDs of the simulated signal in (56), optimised according to the normalised resolution performance measure with higher threshold amplitude.

Table 5 shows the new optimised parameters and the performance measure for these TFDs. The TFDs are shown in Figure 24. The performance measures are generally lower for all TFDs, but performance for the non-CS kernels has decreased the most. This can also be seen in the figures since much more of the cross-term is present in Figures 24a) and c) compared to Figures 24b) and d). The effect of the Doppler restriction is hence more prominent for wider LID kernels. All TFDs suffer from the inner artifacts created by the non-linear component. The LID kernel is always unable to suppress these without suppressing the auto-term itself, see Section 3.3.1.

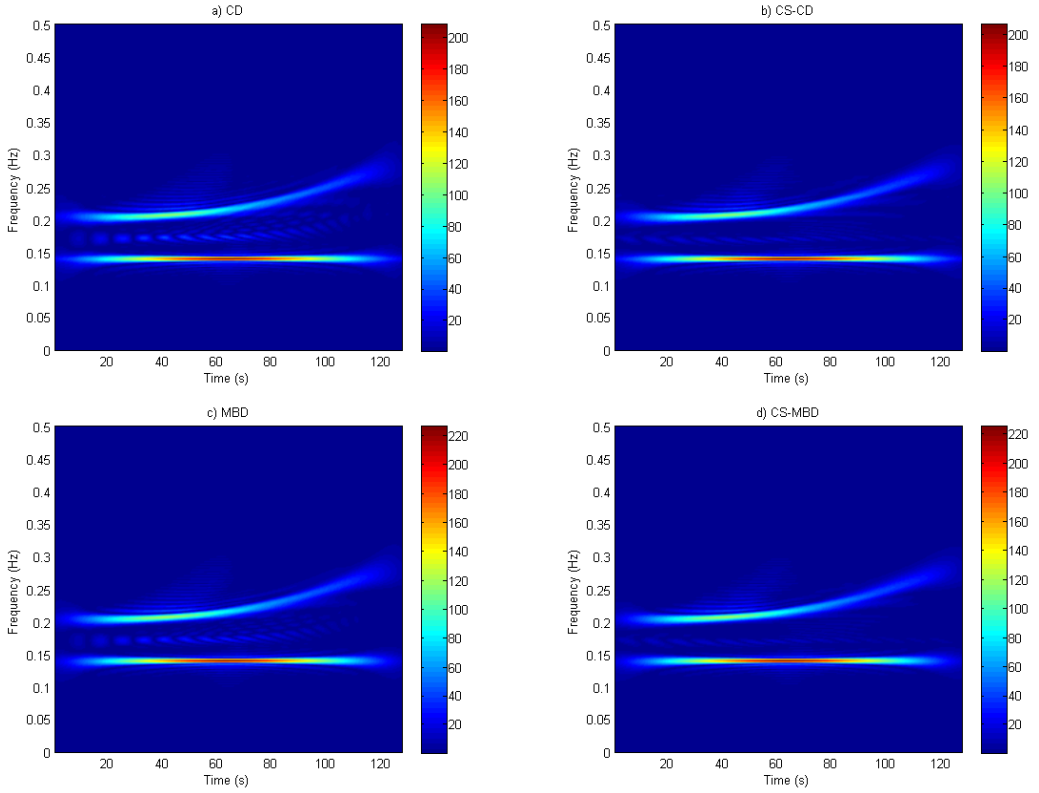

Figure 24: Optimal TFDs of the simulated signal in (56), using the higher threshold amplitude. a) TFD filtered with CD kernel. b) TFD filtered with CS-CD kernel. c)TFD filtered with MBD kernel. d) TFD filtered with CS-MBD kernel.

8 Examples on real HRV data

The HRV signals of 24 patients have been measured while they were breathing according to a metronome with increasing frequency by Jönsson [1]. The increase in respiratory frequency is not linear, which results in a signal resembling the simulated non-linear FM signal in (56). The optimal parameters from the analysis of the TFDs of the simulated signal are in this section used to calculate the TFDs of two patients, only the minimum frequency and Doppler bandwidth are adjusted. The two patients are selected by the criteria that their respiratory frequency resemble the metronome's frequency fairly well. The respiratory signal for the two patients are shown in Figures 25a) and 26a) (lower plots), it can be seen that there are no large and sudden changes in frequency and that the magnitude remains approximately constant. Figures 25a) and 26a) also show the HRV signals (upper plots).

Since the HRV signals are measured, the presence of measurement noise should be considered. If strong noise components exist at one or several frequencies, the signal could not be considered having only two components and additional methods, beyond the interest of this thesis, would be needed to reduce that noise. However the measured HRV signals presented in this section do

[1] Peter Jönsson. Associate professor in psychology. Faculty of Humanities at Kristianstad University

not have any strong measurement noise. This means that the proposed TFDs should show two distinct signal components similar to that of the simulated signals examined in Section 7.

Table 6 shows the parameters used for the different TFDs and their normalised instantaneous resolution performance measures for both patients. The performance measure is calculated using threshold amplitude 0.15 and is calculated only on parts of the TFDs, since it is not possible to automatically identify the correct auto-terms for the whole TFD. The TFD is calculated in the interval 15-150 seconds, where the higher frequency auto-term is strong enough. There is of course an uncertainty in the performance measures, since it is hard, even manually, to determine which peaks are auto-terms. However they can serve as a pointer of the TFDs' performance.

The multitaper TFDs using CD and MBD kernels without penalty function are not presented because their results were very poor. According to the performance measure the TFDs filtered with CD and CS-CD kernels are best for patient 3 and the TFD filtered with the CS-MBD kernel is best for patient 20. However all the TFDs seem to perform equally well. This can also be seen in the Figures, 25b)-h) for patient 3 and 26b)-h) for patient 20, where it is hard to assess the performance of the TFDs. All the TFDs look very similar, the artifacts between the two noticeable signal components are however more smeared for the TFDs using CS kernels and multitapers with suppression.

Looking at the difference between TFDs filtered with CS kernels and non-CS kernels, it can be seen that for these two examples the CS kernels yield about the same results compared to the non-CS kernels. The performance of the multitaper TFDs using the penalty function is not better than all other TFDs, as it was with the simulated signals. This could be due to that the parameters are not optimised for the HRV signals, the very bad performance of the multitaper TFDs not using the penalty function suggest that the multitapers are especially sensitive to tuning.

To get a hint of the performance it is also possible to look manually at time slices. Figure 27 shows the average amplitudes of a few equally spaced time slices in the time interval 1-128 seconds for patient 3. It can be seen that the performance of the CD and CS-CD, Figure 27a), and MBD and CS-MBD, Figure 27b), indeed seem to be similar. However for the peaks in between the two significant components it can be seen that the red line, representing the CS-CD, has lower magnitude than the blue line, representing the CD. The same goes for the MBD and CS-MBD comparison. The plots in Figure 28 shows the same results. The results are still inconclusive but they suggest that improvement might be obtained using the CS kernels and multitapers using penalty for HRV. More testing is of course needed.

TFD	Parameter(s)	Resolution measure patient 3	Resolution measure patient 20
CD	$\gamma = 36$	0.68	0.75
CS-CD	$\gamma = 38$, $\nu_0 = 0.07$	0.68	0.74
Multitaper LB-CD	$\gamma = 96$, $\Delta\nu_p = 0.062$, $P = 20$	0.67	0.74
MBD	$\beta = 0.073$	0.67	0.76
CS-MBD	$\beta = 0.070$, $\nu_0 = 0.07$	0.67	0.77
Multitaper LB-MBD	$\beta = 0.029$, $\Delta\nu_p = 0.062$, $P = 20$	0.66	0.75

Table 6: The normalised instantaneous resolution performance measure for different TFDs of the HRV signal for patients 3 and 20. The threshold amplitude used for the performance measure is 0.15.

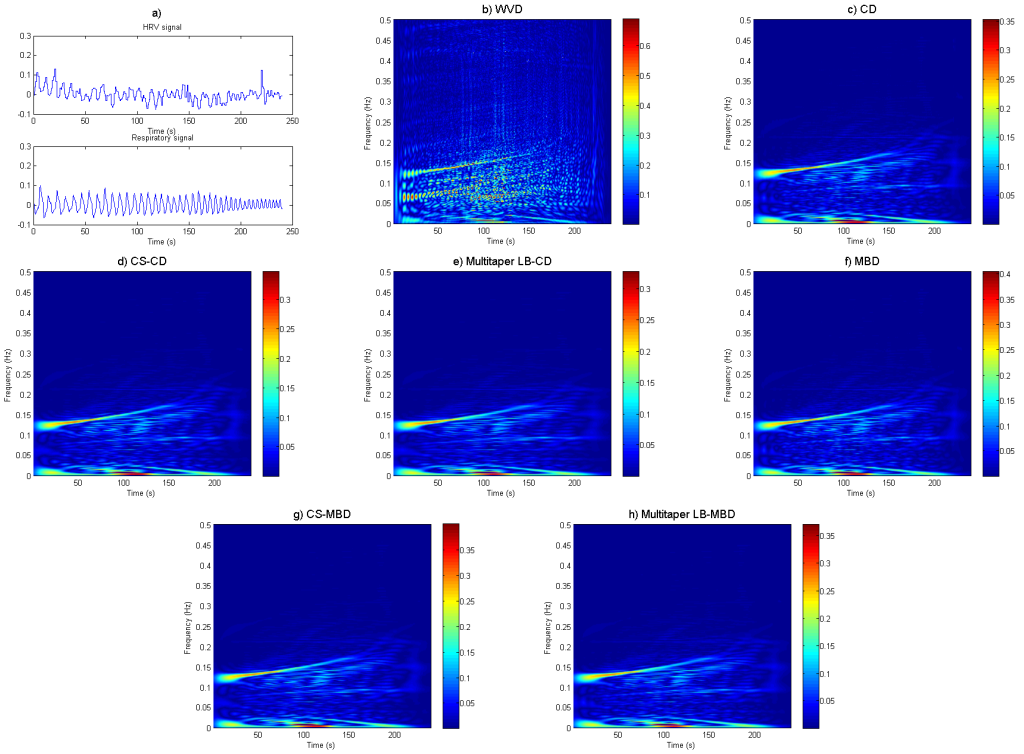

Figure 25: Signal and TFDs for patient 3. a) The HRV and respiratory signals. b) WVD. c) TFD filtered with CD kernel. d) TFD filtered with CS-CD kernel. e) Multitaper TFD using LB-CD kernel. f) TFD filtered with MBD kernel. g) TFD filtered with CS-MBD kernel. h) Multitaper TFD using LB-MBD kernel.

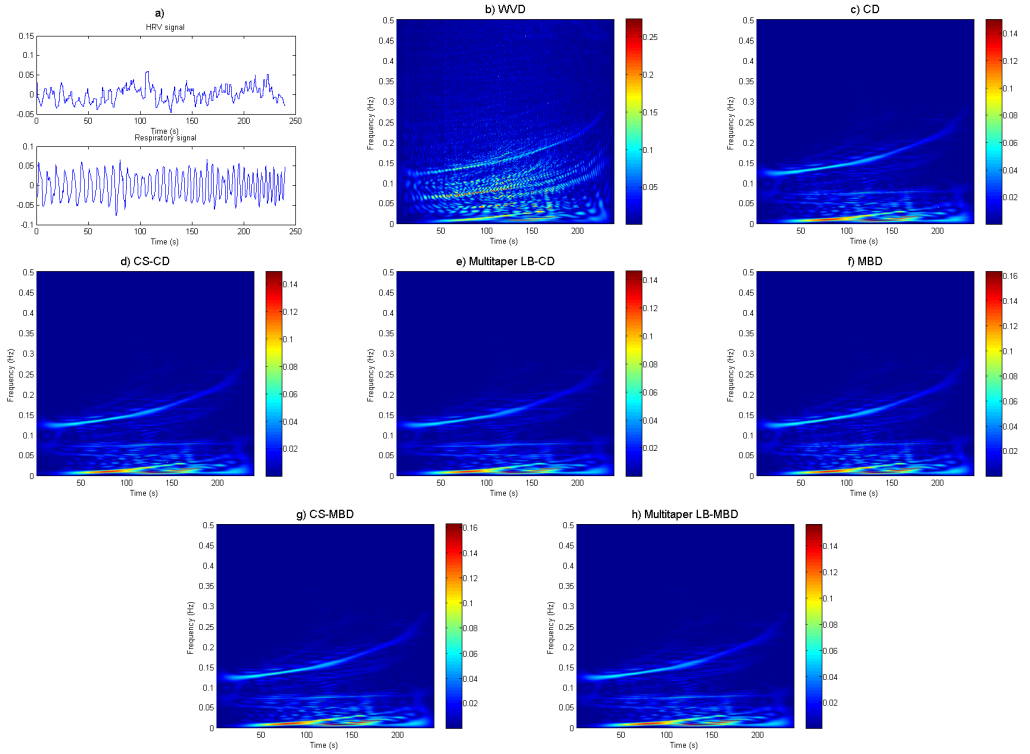

Figure 26: Signal and TFDs for patient 20. a) The HRV and respiratory signals. b) WVD. c) TFD filtered with CD kernel. d) TFD filtered with CS-CD kernel. e) Multitaper TFD using LB-CD kernel. f) TFD filtered with MBD kernel. g) TFD filtered with CS-MBD kernel. h) Multitaper TFD using LB-MBD kernel.

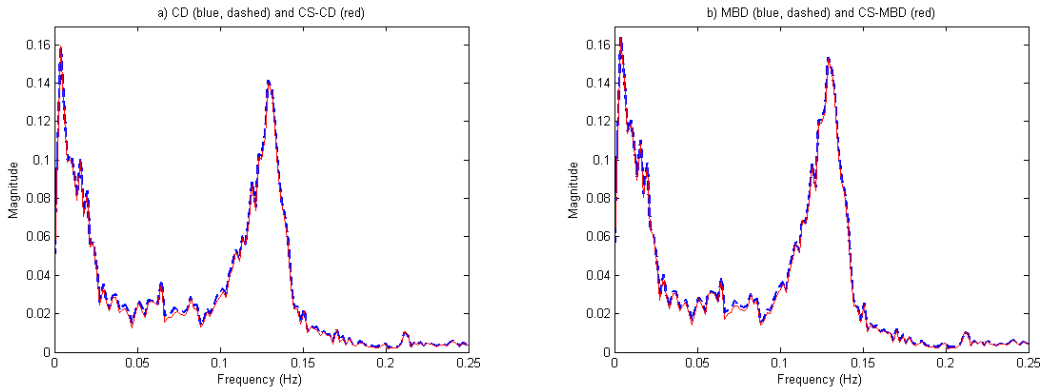

Figure 27: Time slice comparison between the CD and CS-CD TFDs as well as the MBD and CS-MBD for patient 3. The plots are the average of a few equally spaced time slices in the time interval 1-128 seconds.

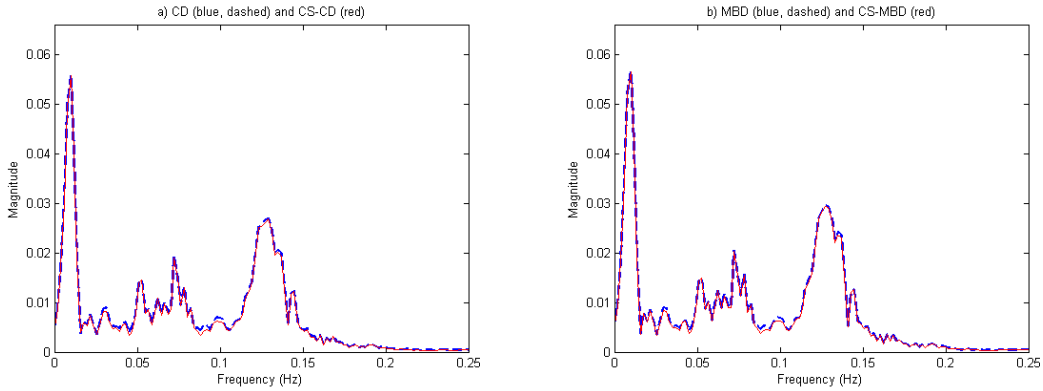

Figure 28: Time slice comparison between the CD and CS-CD TFDs as well as the MBD and CS-MBD for patient 20. The plots are the average of a few equally spaced time slices in the time interval 1-128 seconds.

8.1 Comparison of performance with different threshold amplitudes

The normalised instantaneous resolution performance measure in Table 6 are calculated using threshold amplitude 0.15. This section compares those performance results with the ones obtained when the threshold is 0.10 and 0.30. This will not change the TFD, since the parameters when calculating them are the same, it could however change the performance. If the automatic method calculating the performance identifies the same peaks as auto-terms the performance should be the same or higher for a lower threshold and the same or lower for a higher threshold. The results will thus indicate if the identification is correct and if any TFD suppresses the auto-terms more than the others.

Table 7 shows the performance measures for patient 3, which are the same regardless of threshold amplitude. Table 8 shows the results for patient 20 and there are some differences when the threshold is increased to 0.30. All the performance measures decrease, most with around the same amount, however the multitaper TFD using a CD kernel with penalty function (LB-CD) decreases the most. This probably means that this TFD suppress one of the auto-terms more than the other TFDs.

TFD	Threshold 0.10	Threshold 0.15	Threshold 0.30
CD	0.68	0.68	0.68
CS-CD	0.68	0.68	0.68
Multitaper LB-CD	0.67	0.67	0.67
MBD	0.67	0.67	0.67
CS-MBD	0.67	0.67	0.67
Multitaper LB-MBD	0.66	0.66	0.66

Table 7: The normalised instantaneous resolution performance measure using different threshold amplitudes. The result are shown for 6 different TFDs of the HRV signal for patient 3.

TFD	Threshold 0.10	Threshold 0.15	Threshold 0.30
CD	0.75	0.75	0.65
CS-CD	0.74	0.74	0.64
Multitaper LB-CD	0.74	0.74	0.59
MBD	0.77	0.76	0.65
CS-MBD	0.77	0.77	0.66
Multitaper LB-MBD	0.75	0.75	0.64

Table 8: The normalised instantaneous resolution performance measure using different threshold amplitudes. The result are shown for 6 different TFDs of the HRV signal for patient 20.

9 Conclusions

Two differently distributed LID kernels are used to suppress cross-terms and improve resolution of TFDs of two-component, linear and non-linear, FM signals. The components of the signals also initially have components close in frequency. Two different methods are used to improve resolution and cross-term suppression. These methods, using compact support LID kernels and a multitaper with suppression outside a limited Doppler bandwidth, overall show success increasing performance of the TFDs. The improvement using the CS kernels is most prominent if the distribution of the LID kernel is wider, then any frequency moving auto-term is suppressed minimally. The improvement using suppression outside a Doppler bandwidth for multitaper TFDs is very apparent when compared to ordinary multitaper TFDs for non-linear signals. It is however important to note that optimisations in accordance to different performance measures can yield different optimal TFDs and thus the differences might be less apparent.

The multitaper method with suppression outside a Doppler bandwidth generally performs better than any other method. At least according to the normalised instantaneous resolution performance measure. The disadvantage with this method is however that several parameters need to be optimised and that its performance is sensitive to the chosen parameters for a given signal. There is no Doppler bandwidth which always performs better nor any suppression level. The

optimisation is thus more complex and time consuming compared to the other methods, this means that the method will not be possible to use in some applications.

It is difficult to say if the methods of CS kernels or multitapers with the penalty function can improve TFDs of HRV signals. The analysis on the simulated non-linear FM signal suggests that they could, but the results on the real data are too inconclusive. To get more reliable results more HRV signals need to be tested and some optimisation of the TFDs needs to be done.

Two altogether different performance methods have been presented and used. Optimisation with respect to these yielded very different TFDs. One of the methods also had to be modified to ensure that the desired characteristics were benefited when calculating the performance. This shows how hard it is to objectively assess the performance of different TFDs. The desired characteristics often depend on the application and any performance measure used must reflect this, while still remaining objective.

The proposed improved method of automatically detecting auto- and cross-terms does successfully identify the correct auto-terms of the simulated signals. The detection for WVDs is much improved with this method compared to the original method. It also performs better for some non-linear FM signals where the original method failed. The improved method however does not always detect the correct auto-terms for the real HRV signals, but neither does the original method.

10 Further work

This thesis shows that the methods using CS kernels and multitapers with penalty function improve TFDs for linear and non-linear FM signals. The methods are also tested on HRV data, however since only two examples are used, it is impossible to make any conclusions on the performance of the methods for these signals. Further testing with larger data sets is needed to draw any conclusions. Some optimisation for the TFDs of the HRV signals also need to be done in order to get useful results. The method of performance evaluation for these tests should also be considered. The methods for performance evaluation used in this thesis need to be extended.

A Calculation of TDF for a signal with two frequency components using a LID kernel

Multiplication of the lag-independent, Cauchy kernel

$$G_{\mathrm{cd}}(\nu) = e^{-\gamma|\nu|}, \tag{57}$$

with the ambiguity function

$$A_{z_1}(\nu,\tau) = \delta(\nu)\left(e^{i2\pi f_0\tau} + e^{i2\pi f_1\tau}\right) + \left(\delta(\nu+(f_0-f_1)) + \delta(\nu-(f_0-f_1))\right)e^{i\pi(f_0+f_1)\tau}, \tag{58}$$

of the signal, $z_1(t) = e^{i2\pi f_0 t} + e^{i2\pi f_1 t}$, yields

$$\begin{aligned} G_{\mathrm{cd}}(\nu)A_{z_1}(\nu,\tau) = \delta(\nu)e^{-\gamma|\nu|}&\left(e^{i2\pi f_o\tau} + e^{-2\pi f_1\tau}\right) \\ &+ \Big(\delta(\nu+f_0-f_1) + \delta(\nu-f_0+f_1)\Big)e^{-\gamma|\nu|}e^{i\pi(f_0+f_1)\tau}, \end{aligned} \tag{59}$$

It is thus possible to calculate the TFD for the auto and cross-terms separately, which also means that it is possible to integrate over ν and τ separately.

The integration over ν for the auto-term is

$$\int_{-\infty}^{\infty} \delta(\nu)e^{-\gamma|\nu|}e^{i2\pi t\nu}d\nu = 1. \tag{60}$$

One of the cross-terms becomes

$$\begin{aligned} &\int_{-\infty}^{\infty} \delta(\nu+f_0-f_1)e^{-\gamma|\nu|}e^{i2\pi t\nu}d\nu \\ &= e^{-\gamma|f_0-f_1|}e^{-i2\pi(f_0-f_1)t}, \end{aligned} \tag{61}$$

and the integration for the other cross-term is very similar

$$\begin{aligned} &\int_{-\infty}^{\infty} \delta(\nu-f_0+f_1)e^{-\gamma|\nu|}e^{i2\pi t\nu}d\nu \\ &= e^{-\gamma|f_0-f_1|}e^{i2\pi(f_0-f_1)t}. \end{aligned} \tag{62}$$

Lets now integrate over τ. For the two terms connected to the auto-terms the following is obtained

$$\int_{-\infty}^{\infty} e^{i2\pi f_0\tau}e^{-i2\pi f\tau}d\tau = \int_{-\infty}^{\infty} e^{i2\pi(f_0-f)\tau}d\tau = \delta(f-f_0), \tag{63}$$

$$\int_{-\infty}^{\infty} e^{i2\pi f_1\tau}e^{-i2\pi f\tau}d\tau = \int_{-\infty}^{\infty} e^{i2\pi(f_1-f)\tau}d\tau = \delta(f-f_1). \tag{64}$$

The integration for the cross-term is similar

$$\int_{-\infty}^{\infty} e^{i\pi(f_0+f_1)\tau}e^{-i2\pi f\tau}d\tau = \int_{-\infty}^{\infty} e^{i2\pi\left(\frac{f_0+f_1}{2}-f\right)\tau}d\tau = \delta\left(f-\tfrac{f_0+f_1}{2}\right). \tag{65}$$

The only thing remaining is to add and multiply the correct terms to get the TFD of the LID kernel and signal $z_1(t)$. The resulting TFD is

$$\begin{aligned}
&\int_{-\infty}^{\infty}\int_{-\infty}^{\infty} g(\nu)A_x(\nu,\tau)e^{-i2\pi(\tau f-\nu t)}d\tau d\nu \\
&= \delta(f-f_0)+\delta(f-f_1)+\delta\left(f-\tfrac{f_0+f_1}{2}\right)e^{-\gamma|f_0-f_1|}\left(e^{i2\pi(f_0-f_1)t}+e^{-i2\pi(f_0-f_1)t}\right) \\
&= \delta(f-f_0)+\delta(f-f_1)+2\delta\left(f-\tfrac{f_0+f_1}{2}\right)e^{-\gamma|f_0-f_1|}\cos(2\pi(f_0-f_1)t).
\end{aligned} \tag{66}$$

B Calculation of TDF for a signal with two time components using a LID kernel

The LID kernel in time domain is

$$g_{\mathrm{cd}}(t) = \frac{\left(\gamma^2 + 4\pi^2 t^2\right)^{-1}}{\int_{-\infty}^{\infty} \left(\gamma^2 + 4\pi^2 \xi^2\right)^{-1} d\xi}, \tag{67}$$

and the WVD of the signal $z_2(t) = \delta(t - t_0) + \delta(t - t_1)$ is

$$W_{z_2}(t, f) = \delta(t - t_0) + \delta(t - t_1) + 2\delta\left(t - \tfrac{t_0+t_1}{2}\right) \cos\left(2\pi f \tfrac{t_0+t_1}{2}\right). \tag{68}$$

The filtered TFD is then calculated by a convolution in time

$$\begin{aligned} \rho_{z_2}(t, f) &= g_{\mathrm{cd}}(t) \underset{t}{*} W_{z_2}(t, f) \\ &= \int_{-\infty}^{\infty} \frac{\left(\gamma^2 + 4\pi^2 u^2\right)^{-1}}{\int_{-\infty}^{\infty} \left(\gamma^2 + 4\pi^2 \xi^2\right)^{-1} d\xi} \Big(\delta(u - t - t_0) + \delta(u - t - t_1) \\ &\quad + 2\delta\left(u - t - \tfrac{t_0+t_1}{2}\right) \cos\left(2\pi f \tfrac{t_0+t_1}{2}\right) \Big) du. \end{aligned} \tag{69}$$

Noting that there are several terms which do not depend on u it is sufficient to calculate the following convolutions

$$\int_{-\infty}^{\infty} \delta(u - t - t_0) \left(\gamma^2 + 4\pi^2 u^2\right)^{-1} du = \left(\gamma^2 + 4\pi^2 (t - t_0)^2\right)^{-1}, \tag{70}$$

$$\int_{-\infty}^{\infty} \delta(u - t - t_1) \left(\gamma^2 + 4\pi^2 u^2\right)^{-1} du = \left(\gamma^2 + 4\pi^2 (t - t_1)^2\right)^{-1}, \tag{71}$$

$$\int_{-\infty}^{\infty} \delta\left(u - t - \tfrac{t_0+t_1}{2}\right) \left(\gamma^2 + 4\pi^2 u^2\right)^{-1} du = \left(\gamma^2 + 4\pi^2 \left(t - \tfrac{t_0+t_1}{2}\right)^2\right)^{-1}. \tag{72}$$

This then gives the following TFD

$$\begin{aligned} \rho_{z_2}(t, f) = &\frac{\left(\gamma^2 + 4\pi^2 (t - t_0)^2\right)^{-1} + \left(\gamma^2 + 4\pi^2 (t - t_1)^2\right)^{-1}}{\int_{-\infty}^{\infty} \left(\gamma^2 + 4\pi^2 \xi^2\right)^{-1} d\xi} \\ &+ \frac{2\left(\gamma^2 + 4\pi^2 \left(t - \tfrac{t_0+t_1}{2}\right)^2\right)^{-1} \cos\left(2\pi f \tfrac{t_0+t_1}{2}\right)}{\int_{-\infty}^{\infty} \left(\gamma^2 + 4\pi^2 \xi^2\right)^{-1} d\xi}. \end{aligned} \tag{73}$$

References

[1] Gary G. Berntson et al. 1997. 'Heart rate variability: Origins, methods, and interpretive caveats'. *Psychophysiology*, vol. 34, pp. 623-648.

[2] M. Terese Verklan and Nikhil S. Padhye. 2004. 'Spectral Analysis of Heart Rate Variability: An Emerging Tool for Assessing Stability During Transition to Extrauterine Life'. *JOGNN*, vol. 34, pp. 256-265.

[3] Valentina Magagnin et al. 2011. 'Non-stationarities significantly distort short-term spectral, symbolic and entropy heart rate variability indices'. *Physiol. Meas.*, vol. 32, pp. 1775–1786.

[4] Boualem Boashash. 2003. 'Time-Frequency Concepts' in *Time Frequency Signal Analysis and Processing - A Comprehensive Reference*, Boualem Boashash. Elsevier Ltd, Oxford, 1st edition, ch. 1, pp. 3-27.

[5] Boualem Boashash. 2003. 'Theory of Quadratic TFDs' in *Time Frequency Signal Analysis and Processing - A Comprehensive Reference*, Boualem Boashash. Elsevier Ltd, Oxford, 1st edition, ch. 3, pp. 59-81.

[6] William J. Williams. 2003. 'Reduced Interference Time-Frequency Distributions' in *Time Frequency Signal Analysis and Processing - A Comprehensive Reference*, Boualem Boashash. Elsevier Ltd, Oxford, 1st edition, ch. 5.2, pp. 168-177.

[7] Maria Sandsten. 2013. *Time-Frequency Analysis of Non-Stationary Processes - An Introduction*. Lund University, Centre of Mathematical Sciences, Lund.

[8] Boualem Boashash. 2003. 'Heuristic Formulation of Time-Frequency Distributions' in *Time Frequency Signal Analysis and Processing - A Comprehensive Reference*, Boualem Boashash. Elsevier Ltd, Oxford, 1st edition, ch. 2, pp. 29-57.

[9] Patric Flandrin. 2003. 'Cross-Terms & Localization in Quadratic Time-Frequency Distributions' in *Time Frequency Signal Analysis and Processing - A Comprehensive Reference*, Boualem Boashash. Elsevier Ltd, Oxford, 1st edition, ch. 4.2, pp. 94-101.

[10] Shiying Dong, Ghasem Azemi, Boualem Boashash. 2013. 'Improved characterization of HRV signals based on instantaneous frequency features estimated from quadratic time–frequency distributions with data-adapted kernels'. *Biomedical Signal Processing and Control*, vol. 10, pp. 153–165.

[11] David J. Thomson. 1982. 'Spectrum estimation and harmonic analysis'. *Proceedings of the IEEE*, vol. 70, pp. 1055-1096.

[12] Leon Cohen. 1995. *Time-Frequency Analysis*. Prentice-Hall.

[13] Maria Hansson-Sandsten. 2010. 'Multitaper Wigner and Choi-Williams distributions with predetermined Doppler-lag bandwidth and sidelobe supression'. *Signal Processing*, vol. 91, pp. 1457-1465.

[14] Boualem Boashash, Victor Sucic. 2003. 'Resolution measure criteria for the objective assessment of the performance of quadratic time-frequency distributions'. *Signal Processing*, vol. 51, pp. 1253 - 1263.

[15] Victor Sucic, Boualem Boashash. 2001. 'Parameter selection for optimising time-frequency distributions and measurements of time-frequency characteristics of non-stationary signals'. *Proc. IEEE Int. Conf. Acoust., Speech, Signal Process.*, vol. 6, pp. 3557 - 3560.

[16] Victor Sucic, Boualem Boashah. 2001. 'Optimisation algorithm for selecting quadratic time-frequency distributions: Performance results and calibration'. *Signal Processing and its Applications*, vol. 1, pp. 331-334.